



Terahertz Metasurfaces: Toward Multifunctional and Programmable Wave Manipulation

Han Wei Tian, Hai Yang Shen, Xin Ge Zhang, Xin Li, Wei Xiang Jiang* and Tie Jun Cui*

State Key Laboratory of Millimeter Wave, Department of Radio Engineering, Southeast University, Nanjing, China

OPEN ACCESS

Edited by:

Sreekanth Kandammathe Valiyaveedu,
Nanyang Technological
University, Singapore

Reviewed by:

Jining Li,
Tianjin University, China
Yogesh Kumar Srivastava,
Nanyang Technological
University, Singapore

*Correspondence:

Wei Xiang Jiang
wxjiang81@seu.edu.cn
Tie Jun Cui
tjcui@seu.edu.cn

Specialty section:

This article was submitted to
Optics and Photonics,
a section of the journal
Frontiers in Physics

Received: 16 July 2020

Accepted: 09 September 2020

Published: 23 October 2020

Citation:

Tian HW, Shen HY, Zhang XG, Li X,
Jiang WX and Cui TJ (2020) Terahertz
Metasurfaces: Toward Multifunctional
and Programmable Wave
Manipulation. *Front. Phys.* 8:584077.
doi: 10.3389/fphy.2020.584077

Metasurfaces, composed of prearranged artificial unit cells possessing different electromagnetic (EM) responses, provide unprecedented abilities to realize versatile wave manipulations. Especially in the terahertz spectrum, metasurfaces attract broad attention by opening up further possibilities for wave regulating. Terahertz applications in various fields, for instance, spatial light modulation (SLM), radar, imaging, time-domain spectroscopy (TDS), and high-speed communication, have been facilitated and improved. In this article, we first give a simple review on recent advances on terahertz metasurfaces, including discussion of passive metasurfaces with fixed structures and active metasurfaces integrated with tunable components. Then, we briefly review the development of coding metasurfaces and programmable metasurfaces represented by digitized bits. We mainly focus on some powerful functions, functional multiplexing, and real-time controlled applications in terahertz frequencies. Finally, we give an abbreviated overview of developing terahertz multifunctional metasurfaces and programmable metasurfaces.

Keywords: terahertz metasurface, passive metasurfaces, active metasurfaces, coding and programmable metasurfaces, real-time multifunctional control

INTRODUCTION

Terahertz spectrum, where frequency covers 0.1 to 100 THz (wavelength ranges from 3 μm to 3 mm), has conspicuous distinctions with microwave, millimeter-wave, and optical field. Due to the inclusion of characteristic frequencies of most biological and chemical molecules, abundant biological and material information can be detected [1]. Small attenuation, strong penetration, and high time spectrum signal-to-noise ratio (SNR) also make terahertz wave itself suitable for imaging [2]. In addition, its wide instantaneous bandwidth promotes the implementation of high-speed communication [3]. As these advantages of terahertz spectrum are gradually recognized and accounted, series of terahertz devices have been proposed to regulate terahertz wavefronts [4–6], yet some devices need to face the large volume, high cost, and fabrication issue, which restrict their applications in terahertz scenarios. Distinguished from conventional gratings or phase waveplates, metasurface has played a significant role at terahertz spectrum. As an evolution of three-dimensional (3D) metamaterial in two-dimensional (2D) geometry, metasurface retains advantages in achieving intricate manipulations of electromagnetic (EM) waves that are difficult to realize utilizing conventional technics, while compensating deficiencies of metamaterial such as bulky size, high profile, and difficult fabrication.

Different from metamaterial that is characterized under effective medium theory with retrieved permittivity and permeability [7], generalized sheet transition conditions (GSTCs)

[8], and generalized Snell's laws [9] are fitter for analyzing and designing metasurface. Through permuting artificial and subwavelength metasurface unit cells under characteristic configurations, discontinued phase profiles, arbitrary amplitude profiles, or desired surface impedance distributions can be acquired and one can modulate the incident EM waves at liberty. Hitherto, various metasurfaces have been designed and fabricated to achieve tremendous functions in different physical fields, including acoustic field, microwave and millimeter-wave field, and optical field. Numerous functionalities have been realized, such as high-efficiency transmission [10–12], orbital angular momentum (OAM) generation [13], radar cross section (RCS) reduction [14], and so on. Typically, metasurfaces have been used to construct novel terahertz devices to break volume and cost constraints at terahertz band. Capabilities of manipulating terahertz waves have been enriched and available scenarios have been broadened, such as spatial light modulation (SLM), biological or medical imaging [15], and terahertz time-domain spectrograph [16].

More recently, multifunctional metasurface, coding metasurface, and programmable metasurface turn into research hotspots because of demands of device integration and real-time control. The multifunctional feature gives rise to the advantage of compactness, which may contribute to promoting the miniaturization of terahertz devices or systems. Coding metasurface, of which EM responses are characterized by digitalized bits, provides a direct joint between digital sequences and metasurface. Programmable metasurface is an extended form of coding metasurface, which can activate tunable elements by importing digital coding sequence in the real-time manner, thus realizing dynamic switching of functions. In this article, we intend to review metasurfaces reacting in the terahertz spectrum, of which multifunctional and programmable properties are particularly focused and further regarded as a develop prospect. The organization of this review is as follows. In section Passive Metasurfaces for Terahertz Manipulation, we briefly retrospect several passive metasurfaces aimed for terahertz wave regulating and functional versatility. In section Active Metasurfaces for Terahertz Manipulation, we introduce some terahertz metasurfaces combining activated items to realize tunable responses, while dynamically functional multiplexing is included. In section Coding and Programmable Metasurfaces for Terahertz Manipulation, we review the development of coding metasurfaces and subsequent programmable metasurfaces by listing certain remarkable achievements and real-time controlled cases in terahertz category. In conclusion, we summarize the review along with our prospection on further directions of terahertz metasurfaces with multifunctionality and instantaneity.

PASSIVE METASURFACES FOR TERAHERTZ MANIPULATION

Monofunctional Passive Metasurfaces

In contrast to traditional passive terahertz devices, metasurfaces possess superiorities like ultra-thin profile, remarkable lightness, easy fabrication, acceptable loss, and the tremendous potential

to manipulate terahertz waves freely. Up to now, passive metasurfaces have been utilized to achieve beam deflection [17–19], beam forming [20–22], object cloaking [23], focusing [24–26], absorbing [27], and polarization converting [28–30], and so on. In this part, we focus on the most frequently used functions, for instance, beam deflection and beam forming.

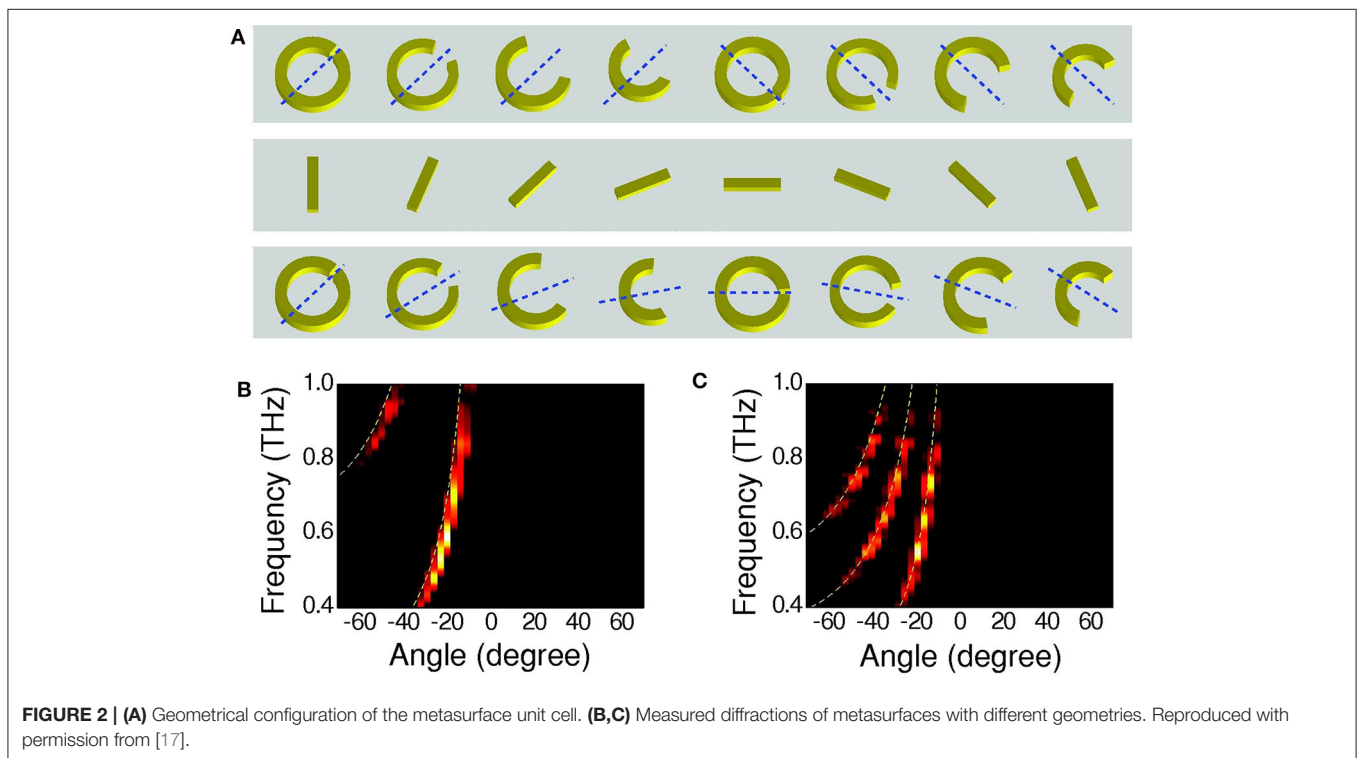
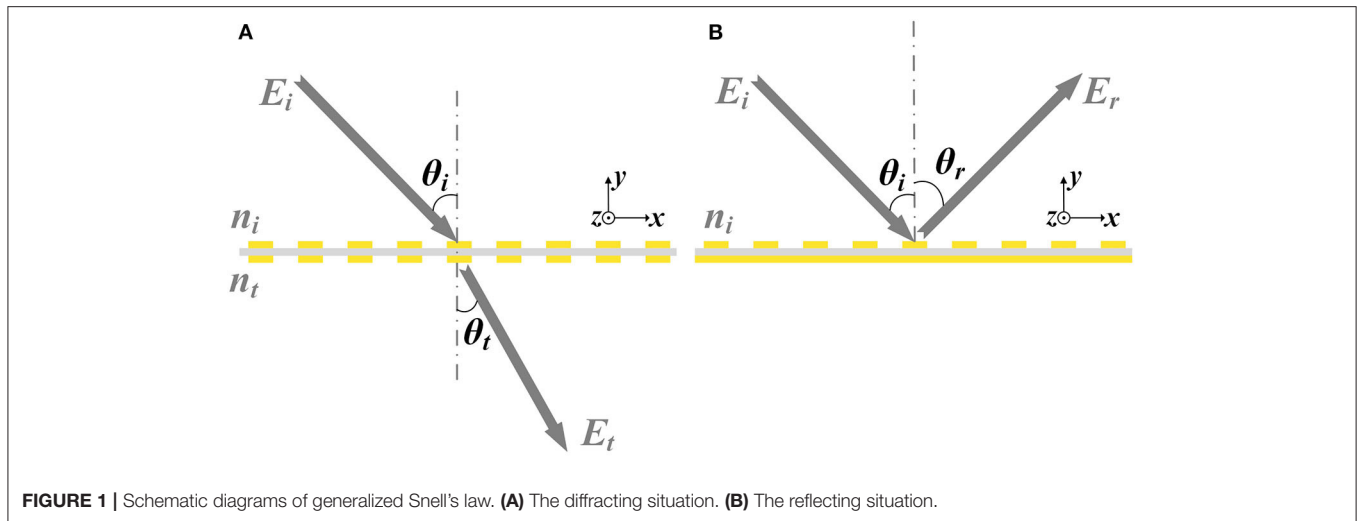
Beam deflection is common and easy to achieve by using conventional technics but need thick terahertz/optical elements or complex light paths. Fortunately, metasurface can be adopted instead to regulate incident waves to expected directions. An external wave vector is applied to the transmitted or reflected wave by etching periodically metasurface unit cells, which realizes the beam deflection effect. According to the generalized Snell's law, a desired diffracting angle θ_t can be achieved under an arbitrary incident angle θ_i ,

$$\sin \theta_t n_t - \sin \theta_i n_i = \frac{\lambda_0}{2\pi} \frac{d\varphi}{dx} \quad (1)$$

in which n_t and n_i are respectively refraction indexes of two media above and underneath the metasurface, as shown in **Figure 1A**. λ_0 is the operating wavelength and $d\varphi/dx$ corresponds to the phase gradient endowed by metasurface. Similarly, in the case of reflection shown in **Figure 1B**, the equation changes to

$$\sin \theta_r - \sin \theta_i = \frac{\lambda_0}{2\pi n_i} \frac{d\varphi}{dx} \quad (2)$$

where θ_t represents the reflection angle. Based on such a principle, many metasurfaces have been proposed to achieve flexible beam deflections. For example, a type of metasurface-based beam deflector composed of C-shaped unit cells was proposed by Zhang et al. [18]. The designed beam deflector was experimentally verified to approach a wide operating frequency range of 0.57 THz (from 0.43 to 1.0 THz); meantime, a maximum deflected angle of 84° was achieved. Moreover, a meta-zone plate was simultaneously proposed using such design method to focus terahertz radiations within a wide frequency band. Soon after, Liu et al. proposed a robust and facile approach to achieve simultaneous control of phase and amplitude in a single-layer metasurface over a broadband frequency range, and untrammled beam diffractions have been achieved [17]. This design combined characteristics of two types of metasurfaces. The metasurface for phase control was determined by the geometrical configuration of each C-shaped unit cell, and the metasurface for amplitude control was realized by angular orientation manipulation of a rod-shaped unit cell, as shown in **Figure 2A**. In such a case, the phase and amplitude of output light can be freely tailored by changing the geometrical configuration of C-shaped unit cells and angular orientation of rod-shaped unit cells, respectively. As a demonstration, the realized metasurface was used to control intensities of different diffraction orders of terahertz waves. Experimental results, illustrated in **Figures 2B,C**, clearly demonstrate the beam diffraction capability of this metasurface. Although the aforementioned two kinds of metasurfaces have outstanding beam deflecting property, the deflection efficiency is excluded



from consideration. Miniaturization of unit cells can restrain spatial dispersion and spurious diffraction that deteriorate the metasurface performance. In 2019, Liu et al. proposed two deeply subwavelength unit cells based on meander lines and meander gaps with a total size of about $1/25$ wavelength, and the latter one was verified to maintain underdamped under the attenuation of metal conductivity [19]. To further demonstrate the feasibility of the meander gap metasurface, a beam deflector sample based on meander gap metasurface was proposed. The authors verified an efficient deflection effect at the diffraction order of -1 with simulated deflection efficiency over 49% around 1 THz.

To achieve a complex EM pattern, the phase distribution, amplitude distribution, or polarization conversion will be more variable than that of beam deflection, and are no longer monotonic gradient situations. Through endowing complex EM responses to the metasurface, optical elements such as deflectors, splitters, and waveplates can be replaced. The system complexity can be reduced and proper shaping effects can be maintained. For example, Lorentz beam can be used in a wide range of scenarios due to its non-diffraction characteristic, yet multiple optical elements are required to generate it. In 2017, Guo et al. demonstrated a radially polarized Lorentz beam under circular

polarized incidences in the terahertz spectrum utilizing a single-layer metasurface composed of cross-shaped unit cells [22]. The schematic diagram of generating Lorentz beam is shown in

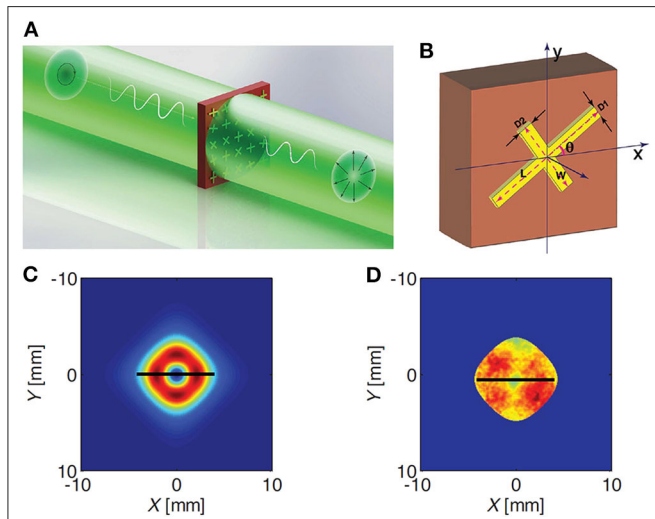


FIGURE 3 | (A) Schematic of the metasurface to generate a radially polarized Lorentz wave from a right circularly polarized uniform plane wave. **(B)** Schematic diagram of the cross-shaped unit cell. Parameters L , W , $D1$, and $D2$ are respectively the length and width of the cross patch. **(C,D)** Simulated and experimental transmitting intensities of the generated Lorentz beam. Reproduced with permission from [22].

Figure 3A. The cross-shaped unit cell, depicted in **Figure 3B**, provides different phase responses, amplitude responses and polarization conversions by modulating typical sizes of the cross pairs and orientation angle θ . Electric field distributions of the metasurface have rotational symmetry with an angle of 90° under two orthogonally circularly polarized (CP) waves (RCP and LCP). Simulated and measured results of total transmitting intensities are respectively depicted in **Figures 3C,D**, from which good compatibility is observed. In addition to Lorentz beam, Bessel beam is another modulated light possessing diffraction-free characteristic. Although ideal Bessel beam only exists in theory, the actual EM radiation obeying formal solution of zero-order Bessel function still exhibits merits like deep focal length, high intensity, and small main-lobe size. Recently, Jia et al. proposed a kind of transmitting metasurface in response to circular polarization and experimentally demonstrated the realization of high-performance Bessel distribution [21]. The authors designed a tri-layer metasurface unit cell with only $\lambda/5$ thickness to provide full phase coverage (0° to 360°) and high transmission. Based on the high-quality unit cell, the generated Bessel beam was verified with outstretched longitudinal field and focused transverse field, satisfying the non-diffracting desire. Besides, OAM beam has also attracted much attention and been regarded as an important way to improve communication capability and information security owing to its infinite orthogonal modes. OAM multiplexing and demultiplexing were demonstrated based on a terahertz metasurface by Zhao et al. and the unit cell

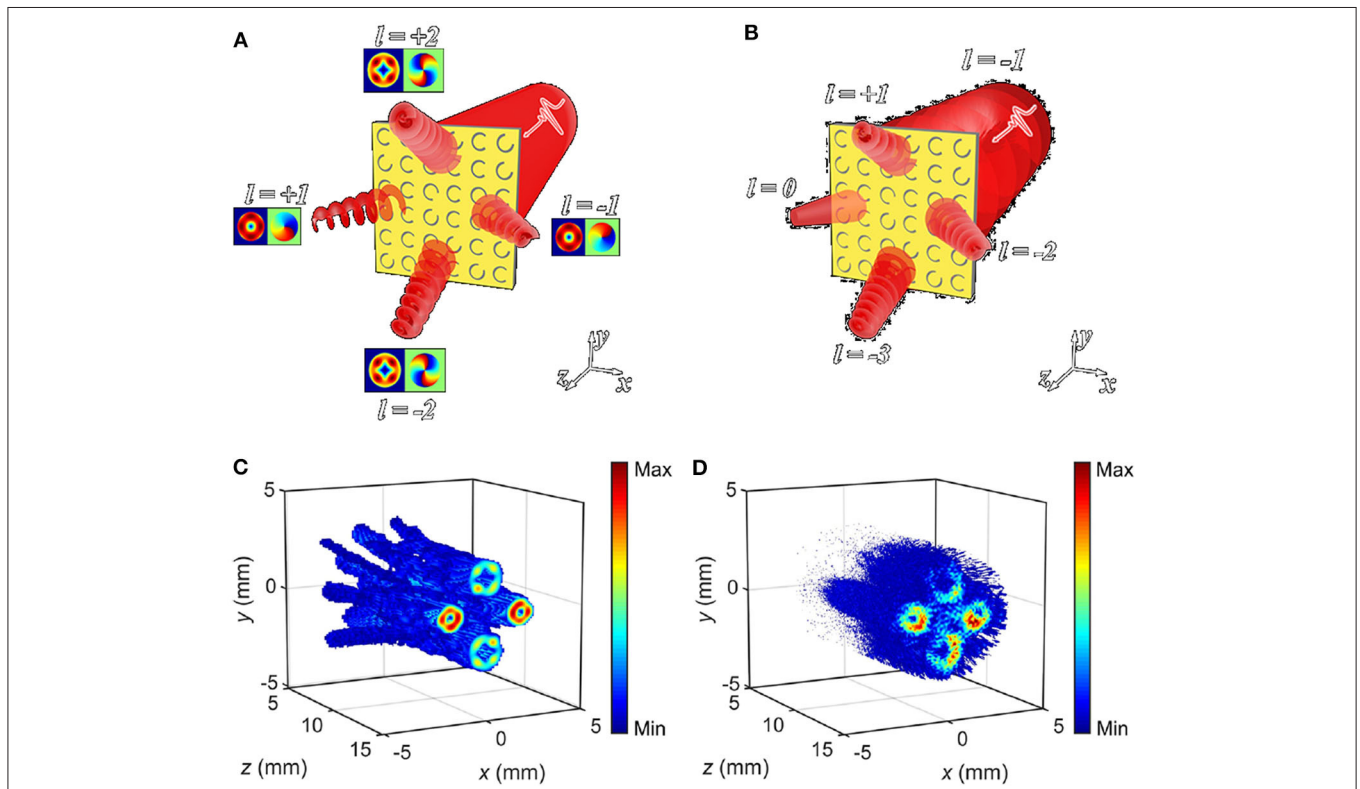
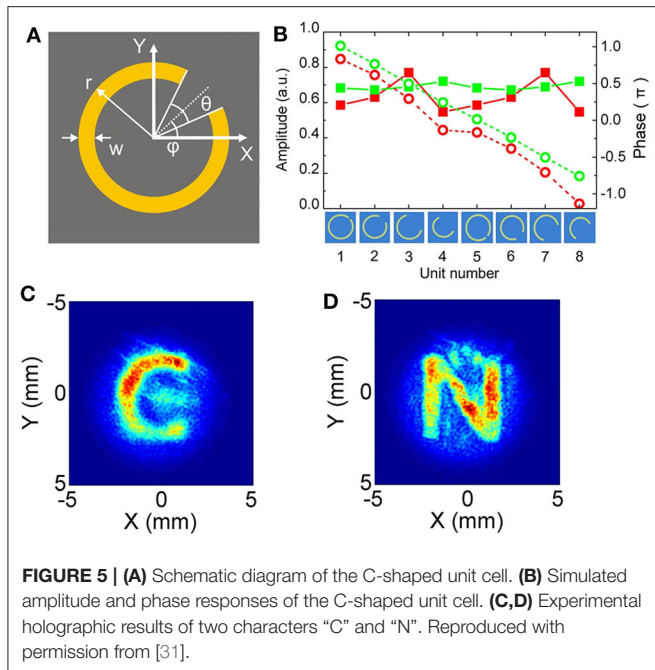


FIGURE 4 | (A,B) Illustration of the metasurface to achieve OAM multiplexing and demultiplexing. **(C,D)** Simulation and experimental amplitude profiles of OAM multiplexing. Reproduced with permission from [20].



was chosen as complementary C-shaped structure [20]. The metasurface structure was designed to multiplex OAM beams with distinct topological charges under the illumination of a Gaussian incidence, and the demultiplexing can be verified by the generation of a focal spot at the desire channel under an individual OAM incidence. Schematics of the metasurface and the corresponding multiplexing and demultiplexing effect are shown in **Figures 4A,B**. By arranging eight types of unit cells with different azimuth angle α and opening angle β , four focused OAM wavefronts with topological charges of $l = +1, -1, +2,$ and -2 were simultaneously realized in simulation and measurement. Then, by entering an OAM beam containing singular topological charge, OAM demultiplexing effect also got demonstration. Simulation and experimental results of OAM multiplexing are depicted in **Figures 4C,D**.

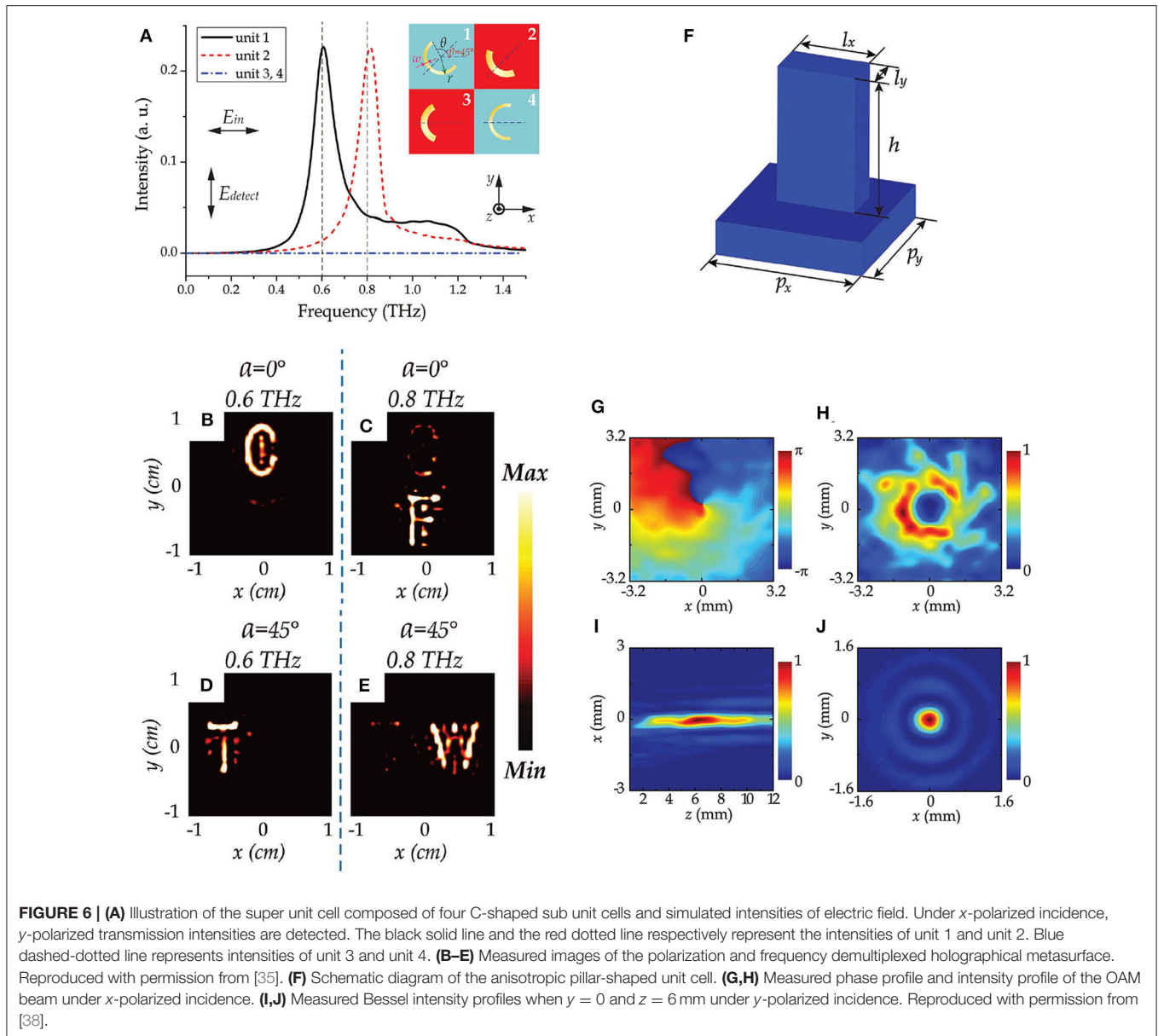
Multifunctional Passive Metasurfaces

In line with the pursuit of high integration and miniaturization, multifunctional devices are undoubtedly one of the current research hotspots. Designing functional devices by traditional methods may be impractical or undesirable ascribing to limitations imposed by their own mechanisms. Fortunately, the superb degree of freedom of metasurface makes functional multiplexing a reality. Although the significant feature of the passive metasurface is its fixed structure, functional multiplexing can still be achieved. Multifunctional passive metasurfaces can be divided into frequency multiplexing metasurfaces [31, 32] and polarization multiplexing metasurfaces [33–38].

We start from the frequency multiplexing situation. Because some metasurface unit cells can function at more than one frequency band, the finally constructed metasurface can realize multiple effects under an overlapping arrangement. As an

example, Wang et al. proposed a multi-color metasurface hologram depending on the phase modulating of C-shaped unit cells effective at different working frequencies [31]. The selected C-shaped unit cell, depicted in **Figure 5A**, can manipulate transmitted phase responses from -180° to $+180^\circ$ at both 0.50 and 0.63 THz, and meanwhile maintain stable amplitude responses. Simulated amplitude and phase responses are illustrated in **Figure 5B**. Utilizing this selected unit cell, the authors designed a metasurface to image recorded hologram characters “C” and “N” respectively at 0.50 and 0.63 THz. Experimental images of two characters are shown in **Figures 5C,D**. Considering the presented images are cross-polarized with respect to the incidence, cross-polarization conversion efficiency of the meta-device was measured with an absolute intensity above 10%. Later in 2018, a bi-functional metasurface structure that could simultaneously achieve anomalous reflection and transmission respectively at dual terahertz bands has been designed and verified [32]. A double-layer metasurface unit cell was firstly presented, in which two C-shaped patterns separately provided reflected and transmitted phase responses. Then, the authors designed a metasurface structure and numerically demonstrated derivation angles of -19.7° for reflection and -50° for transmission.

Furthermore, there are many circumstances belonging to polarization multiplexing. To our knowledge, two principles are commonly employed to design polarization multiplexed metasurfaces, one is Pancharatnam–Berry (PB) phase [33–37] and the other is anisotropy [38]. PB phase can be realized by rotating metasurface unit cell structures, such as the C-shaped structure and rod-shaped structure aforementioned, and there exist a specific relationship between the orientation angle and the PB phase. Values of the PB phase have opposite varying trend under two orthogonal CP incidences when the unit cell rotates, which is crucial for integrating multiple functions. In addition, since unit cell structures based on PB phase do not rely on EM resonances, they are able to maintain stable phase change and amplitude response in wide bands. In 2015, Wang et al. proposed a polarization-dependent metasurface lens originated from PB phase, and a lens prototype was designed and fabricated to achieve different focal spots and disparate character images at different locations [36]. In this work, a rod-shaped unit cell was adopted to provide transmitted PB phase in a wide band. Focal spots were experimentally verified to be diverging under RCP and LCP waves, in the meantime with outstanding focusing effect from 0.65 to 0.95 THz. The lens was also measured with flipped imaging ability under two perpendicular CP incidences. However, the proposed metasurface lens is dominated by the reversal property under different CP illuminations, which constrains the development of functional multiplexing. Fortunately, this issue can be solved by properly designing the cell structure and punching the incidence with specific polarization. For instance, a polarization and frequency demultiplexed holographical metasurface has been designed in terahertz range [35]. Recurring to a super unit cell composed of four C-shaped sub unit cells endowed with different opening angles, orientation angles, and line widths, transmitted polarization conversion intensity and phase response



can be manipulated at multiple frequency points. It is observed in **Figure 6A** that units 1 and 2 achieve y -polarized intensity peaks respectively at 0.6 and 0.8 THz under an x -polarized incidence, but units 3 and 4 have no polarization conversion effect. When rotating the structure to 45° , units 3 and 4 are contributing while units 1 and 2 are inoperative. Then, by using Rayleigh–Sommerfeld diffraction theory, the authors demonstrated a meta-holography possessing the novel functionality to realize polarization selective and frequency selective holographic imaging. Using the multifunctional metasurface, four characters “C,” “F,” “T,” and “W” were chosen to be displayed here, and measured results are shown in **Figures 6B–E**. Furthermore, the idea of polarization multiplexing has been utilized in designing many other powerful meta-devices, such as dual-functional polarization rotator [33] and dual-functional beam generator

[37]. Apart from PB phase, anisotropy is also an effective principle for polarization multiplexing design. Other than the polarization selectivity of PB phase, metasurface structures based on anisotropy rely on polarization independence. To achieve multiple functions, anisotropic unit cell structures that have polarization-independent responses are required. In 2017, Zhang et al. proposed a high-efficiency silicon metasurface consisting of rectangular pillar-shaped unit cells [38]. The unit cell structure is illustrated in **Figure 6F**. Through tuning the side length l_x and l_y , phase shifts corresponding to x polarization and y polarization vary independently. To further demonstrate the anisotropy of the silicon unit cell, the authors designed and fabricated several prototypes of metasurfaces, among which the most conspicuous one was proposed to realize bi-functional beam shaping. Under x -polarized terahertz incidence, this prototype was verified to

serve as an OAM beam generator, while under y -polarized terahertz incidence, the metasurface was verified to generate a Bessel beam. Measured phase profile and field intensities are depicted from **Figures 6G–J**.

ACTIVE METASURFACES FOR TERAHERTZ MANIPULATION

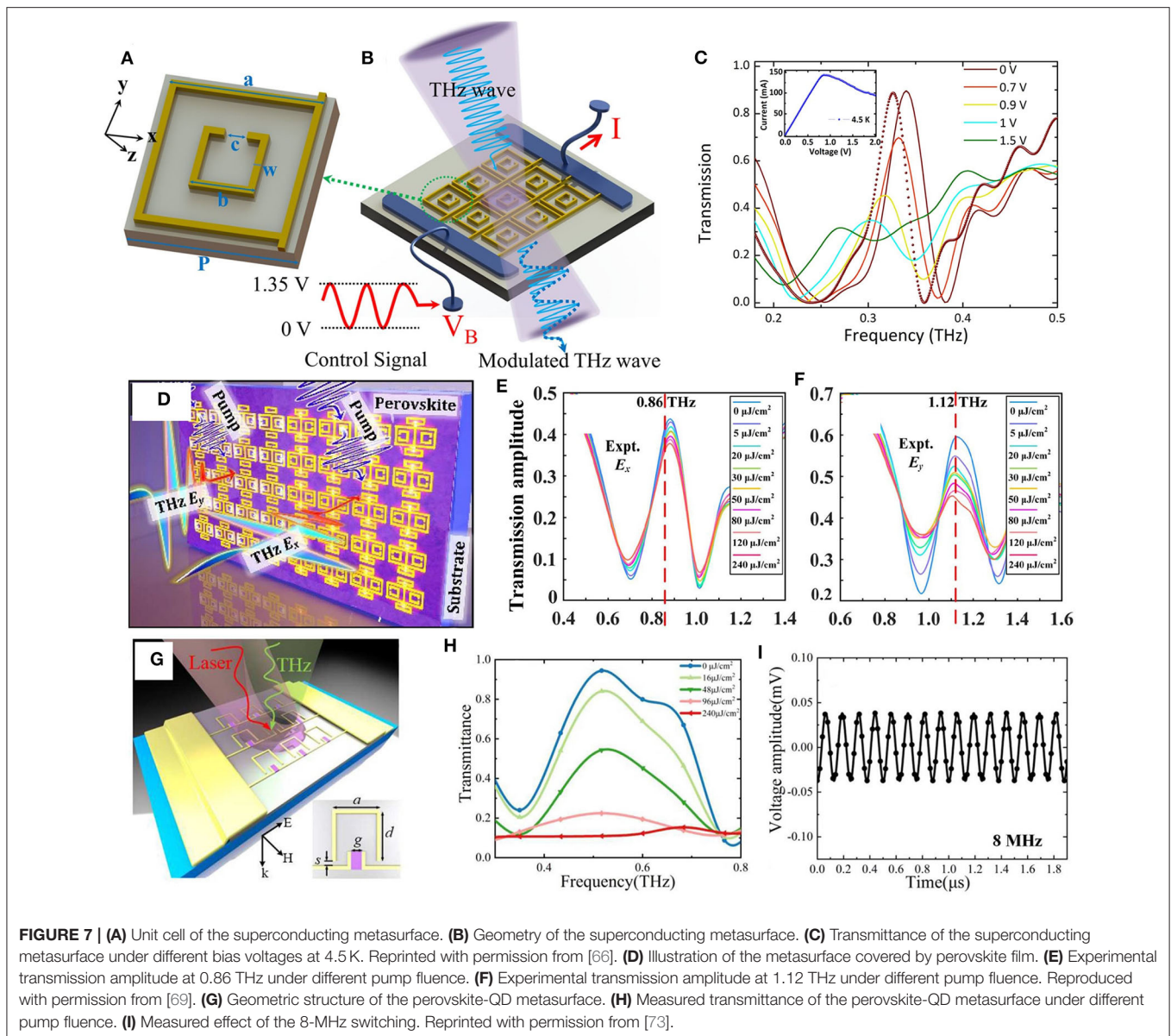
Active Metasurfaces With Functional Tunability

Although functional integration has been realized and widely studied using passive metasurfaces, some intractable situations need active items to perform dynamic control. At microwave frequencies, PIN diodes, varactors, and triodes are widely embraced to provide optional responses under different bias signals, while in the terahertz spectrum, it is difficult to obtain packaged semiconductors owing to the small electrical size, and sophisticated parasitic effects are a formidable challenge. Fortunately, many materials can be utilized as tunable components in terahertz frequencies. Doped semiconductor [39], vanadium dioxide (VO₂) [40], liquid crystal (LC) [41], transparent conducting oxide (TCO) [42], graphene, 2D electron gas (2DEG) [43], halide perovskite [44], quantum dot (QD) [45], and superconductor [46, 47] have been used to design terahertz metasurfaces and experimentally verified with freedom of regulating amplitude responses, phase responses, and polarizations. The excitation method is no longer limited to electric control, and thermal environment and light pump also become effective incentives. Moreover, micro electromechanical systems (MEMS) and nano electromechanical systems (NEMS) are widely adopted to implement dynamic structure adjustment. The former is suitable for terahertz applications, and the latter can be used in near-infrared (NIR) regime [48].

To date, active metasurfaces have been widely used to realize amplitude and/or phase modulation [39, 40, 43–45, 49–76]. Recently, Li et al. proposed an electrically controlled superconducting metasurface to actively tune the transmitting response [66]. As illustrated in **Figures 7A,B**, each unit cell consists of a square-ring resonator and an SRR, which are all made up of superconducting niobium nitride (NbN), and the substrate is chosen as 1 mm MgO. To ensure the superconducting effect, the authors cooled down the environment temperature at 4.5 K. The superconducting metasurface exhibits its ability in tuning the transmittance after being applied different bias voltages. Experimental results, as shown in **Figure 7C**, verified a maximum modulation depth of 79.8% at 0.341 THz when the applied bias voltage is 1 V. The authors also employed sinusoidal AC signal to testify the modulation speed, and the metasurface was demonstrated with a maximum modulation speed of ~ 1 MHz. Soon after, a hybrid perovskite metasurface was proposed for transmittance tuning [69]. The authors first arranged several closed-ring resonators (CRRs) and SRRs to endow the metasurface with polarization sensitivity, and then they covered the metasurface with a 55-nm halide perovskite (CH₃NH₃PbI₃) to make the metasurface photoconductive. The illustration of the metasurface that covers the perovskite film

is shown in **Figure 7D**. As illustrated in **Figures 7E,F**, these CRRs and SRRs introduce Fano resonances at 0.86 THz under x polarization and 1.12 THz under y polarization, and the covered halide perovskite film make the resonances variable under an extra optical pump. When the working fluence of the pump changes from 0 to 240 $\mu\text{J}/\text{cm}^2$, experimental results demonstrate the transmittance tuning ability at two different frequencies with a maximum modulation depth of 25%. Lately, Xiong et al. introduced a new scheme of perovskite-QD metasurface based on inorganic perovskite (CsPbBr₃) under optical excitation and finally realized high-speed switching of terahertz wave [73]. It is clear in **Figure 7G** that the metasurface is composed of periodic SRRs, and the perovskite-QD is embedded at the split of each SRR. Similar to the previous work, optical pumps with different fluence are chosen as driven signals. **Figure 7H** shows the transmittance variation under various laser pump powers. With the pump powers increasing from 0 to 240 $\mu\text{J}/\text{cm}^2$, the transmittance drops from 90 to 10.9% at 0.5 THz. Furthermore, the authors developed the perovskite-QD metasurface to achieve high-speed switching. The authors demonstrated the metasurface as an effective switch with different speeds of 10 KHz and 8 MHz, and the measured 8-MHz switching effect is depicted in **Figure 7I**.

Besides, metasurfaces have been utilized to realize dynamic lenses in response to the demands of varifocal applications [41, 77–80]. In 2017, Huang et al. proposed a graphene-based metasurface lens that can tune the focusing length continually by 1.25λ [78]. The metasurface lens consisted of top gold film etched with rod-shaped slot patterns and bottom substrate containing quartz and silicon, with graphene sheet sandwiched. As a monolayer carbon structure arranged in honeycomb lattice, its intriguing merits are not limited to the ultrathin profile, and controllable optical properties under chemical doping or electrical gating are also attractive. By tuning the chemical potential from 0.1 to 0.3 eV, the authors numerically demonstrated that the focal length decreased from 4.4 to 3.9 mm, with a total shift of 0.5 mm. The authors also demonstrated an acceptable performance tolerance under incidences $< \pm 10^\circ$. Later, Liu et al. modified this lens and further extended it to experiment verification [79]. In such a work, graphene was deposited above the patterned gold film, as shown in **Figure 8A**. Through applying gate voltage to two electrodes attached to the gold film and graphene separately, chemical potential of graphene can be tuned; thus, phase profiles of the lens change correspondingly. In the experiment, the incident wave was centered at 0.75 THz, and two gate voltages 0 and 2 V were applied to the electrodes to explore the varifocal property. As shown in **Figures 8B,C**, the focal length is 12.24 mm when gate voltage is 2.0 V. When the electrodes are suspended, the focus is changed with a shift of 1.78 to 10.46 mm. After applying an adjustable gate voltage between 0 and 2 V, the proposed lens can achieve an outstanding varifocal range of $\sim 4.45\lambda$. Apart from varifocal applications, metasurface lenses have also been utilized to focal scanning. Roy et al. proposed a MEMS-integrated metasurface lens for low angular focus displacements [77]. The lens is passive and rotates under the traction of the MEMS system, so it has lower ohmic loss than other active lenses based

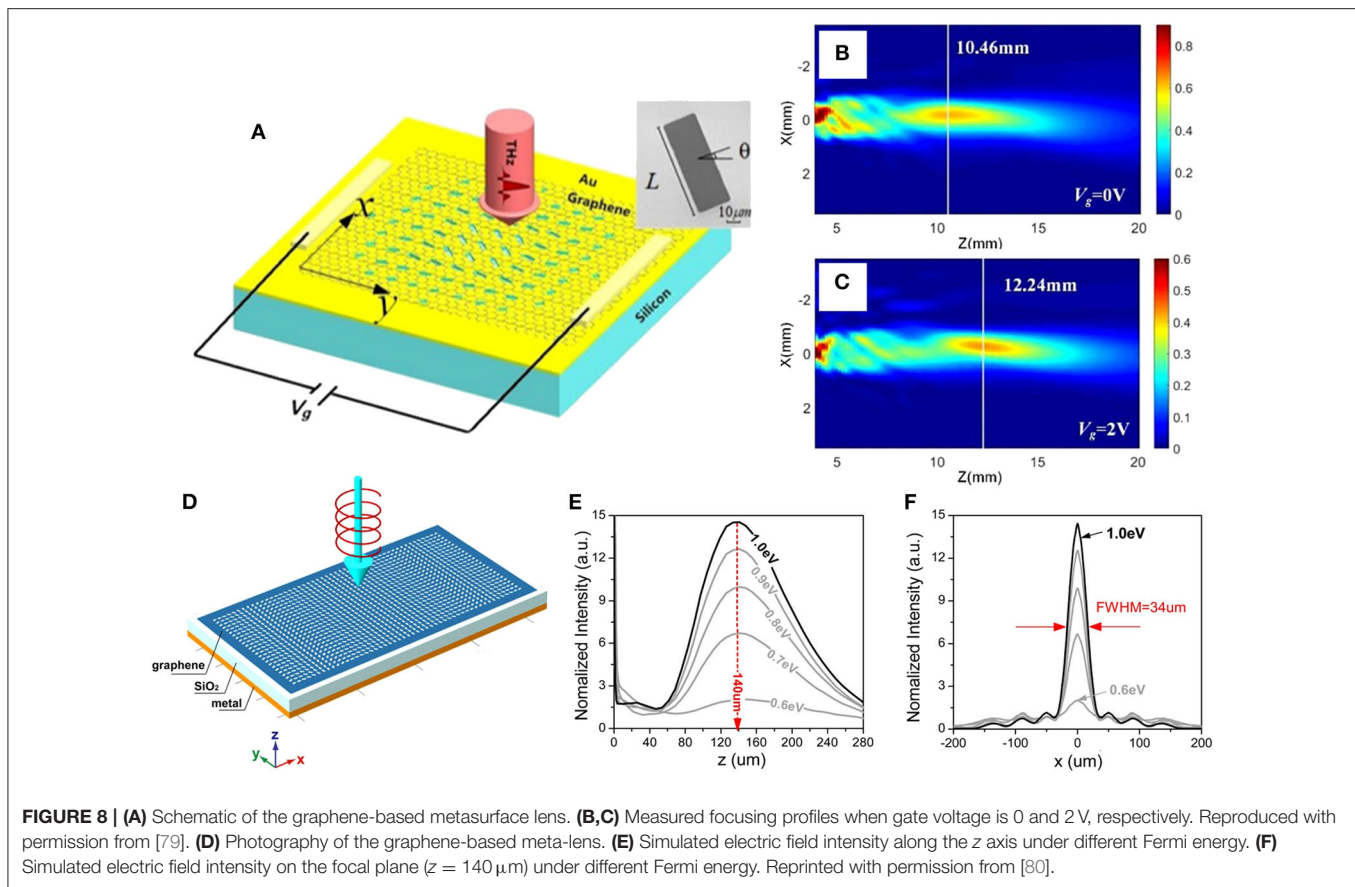


on active materials. To verify the focal scanning property, a collimated Gaussian incidence was illuminated on the scanner at an oblique angle of 45° . Under two actuating voltages of 40 and 60 V, the lens was measured with the focus scanning from 2.7° to 7.3° . The lens-on-MEMS scanner exhibited a stable tunability with an averaged measurement deviation of 0.2%, manifesting a strong practicality. More recently, Ding et al. proposed another graphene-based meta-lens to achieve focusing modulation [80]. The metasurface was composed of a graphene layer perforated with rectangular unit cells, a SiO_2 substrate, and a metal ground, as illustrated in **Figure 8D**. The authors first demonstrated that the meta-lens can achieve efficient focusing effect with a designed focal length of $140 \mu\text{m}$ at 5 THz. Then, by uniformly reducing the Fermi energy of the graphene layer from 1 to 0.6 eV, the intensity at the focal point can be distinctly decreased without perturbing the focal position. As depicted in **Figures 8E,F**, the

focusing efficiency changes from 66.6 to 15.8%, and the focal length remains stable at $140 \mu\text{m}$. Further, the authors discussed the meta-lens with distinguished abilities in focal length tuning, wideband focusing, and wide-angle focusing shifting. In addition to the above two functions, active metasurfaces have also been exploited to achieve absorbing [81–83], beam steering [42, 84–87], polarization switching [88, 89], imaging [90], and so on.

Active Metasurfaces With Dynamically Functional Multiplexing

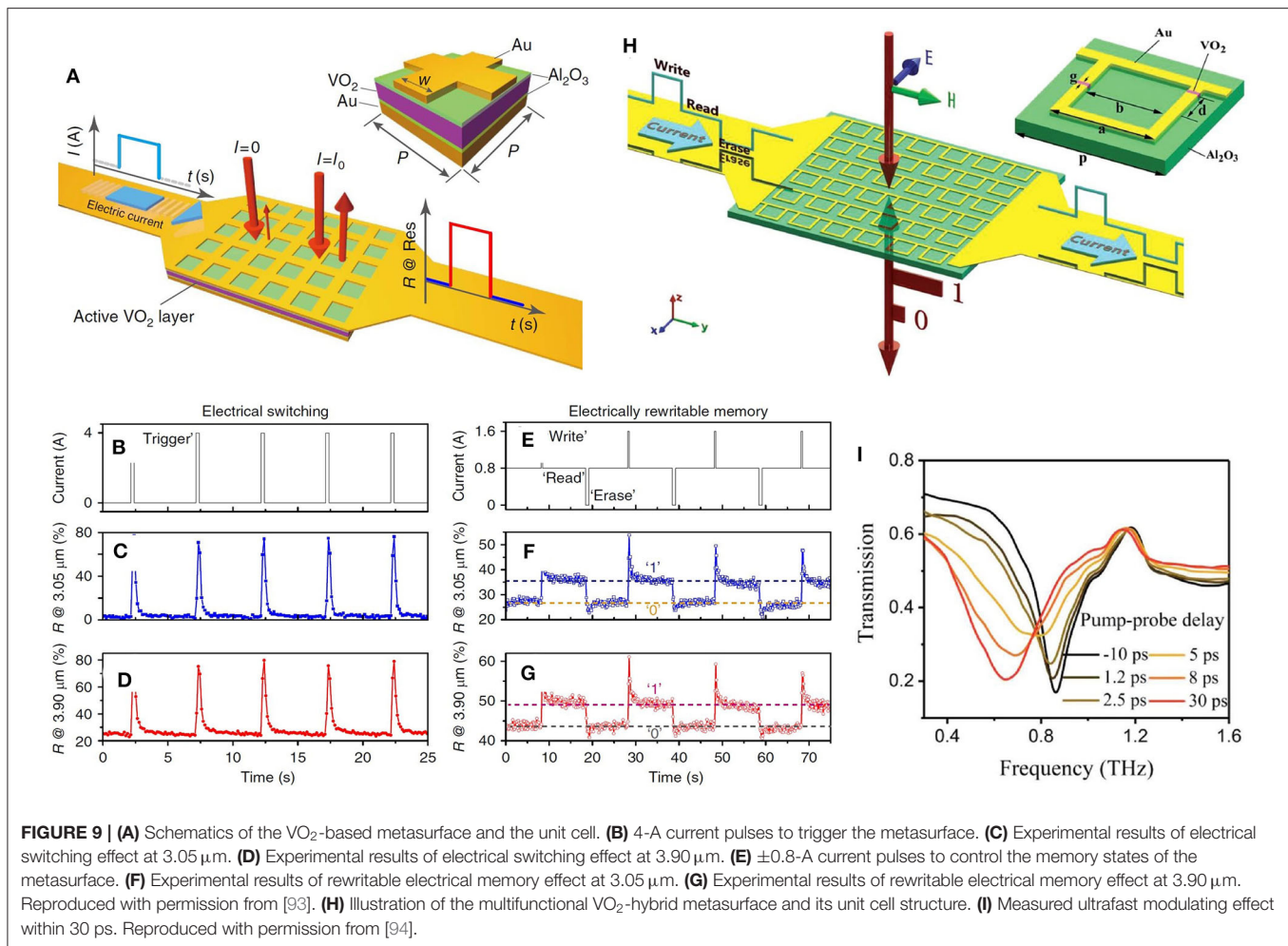
Next, we introduce some metasurfaces that can achieve functional multiplexing dynamically. Making functional multiplexing dynamical can further improve the integration level of various devices and systems, but facing design and manufacturing difficulties is inevitable. In the terahertz and optical spectrum, tiny dimensions and immature technics result



in the functional multiplexing facing great difficulties. Although more hardships are confronted compared to merely achieving function tuning, some active metasurfaces with dynamically functional multiplexing have still been implemented [91–96].

For instance, Liu et al. have realized a kind of VO_2 -based metasurface that can be regarded as electrical switching or rewritable memory [93]. By means of the insulator-to-metal transition (IMT) property of a VO_2 substrate, as shown in **Figure 9A**, current-dependent reflectance of the presented unit cell can be realized in thermal equilibrium, and electrically triggered multifunctional control is expected in an achievable extent. Furthermore, the authors developed the metasurface as a multifunctional meta-platform with potentials as electrical switching and rewritable memory. Both two functions rely on predefined reflectance as thresholds, and different current pulses are employed as trigger signals. By giving the metasurface a 4.0-A electrical pulse with a width of 0.25 s, the meta-platform showed good switching effects at both 3.05 and $3.9 \mu\text{m}$ with rising and falling edge of ~ 0.2 and ~ 0.5 s, as depicted from **Figures 9B–D**. Then, by changing the height of the trigger signal to ± 0.8 A, the meta-platform can serve as a rewritable memory device, and the measured results are depicted from **Figures 9E–G**. More recently, Cai et al. proposed a kind of multifunctional VO_2 -hybrid metasurface also based on IMT [94], as illustrated in **Figure 9H**. In addition to switching and rewritable memory

driven by current pulse, the authors also demonstrated the metasurface with the property of ultrafast modulation under laser pulse excitation. The measured transmissions under different pump-probe delays, as shown in **Figure 9I**, demonstrate the metasurface with tremendous potential for ultrafast modulation within 30 ps. The amplified femtosecond laser pulse brings the modulation speed to picosecond level in contrast to the electrical control in second level. Beyond the multiplexing of information processing functions, there exist active metasurfaces that can multiplex different EM functions, such as beam deflection and holography. For example, Cong et al. discussed the multifunctional property of a MEMS-based metasurface extended to 1D and 2D control [91]. The MEMS-based unit cell was chosen to be a cantilever structure linked with bias lines. By extending the dimension of bias control to 1D, the authors exhibited a beam deflecting function with a deflection angle easily achieved at $\pm 70^\circ$. The authors further designed an array with identical unit cells connected with more complicated bias lines that can perform 2D bias control. With tunable 2D phase profiles, a real-time rewritable holography was numerically demonstrated and two holographic images were generated with overall efficiency larger than 25%. In the same year, a tunable meta-lens that can simultaneously conduct focus shifting and aberration control was proposed [96]. Different from MEMS relying on structural displacements realized by electrostatic



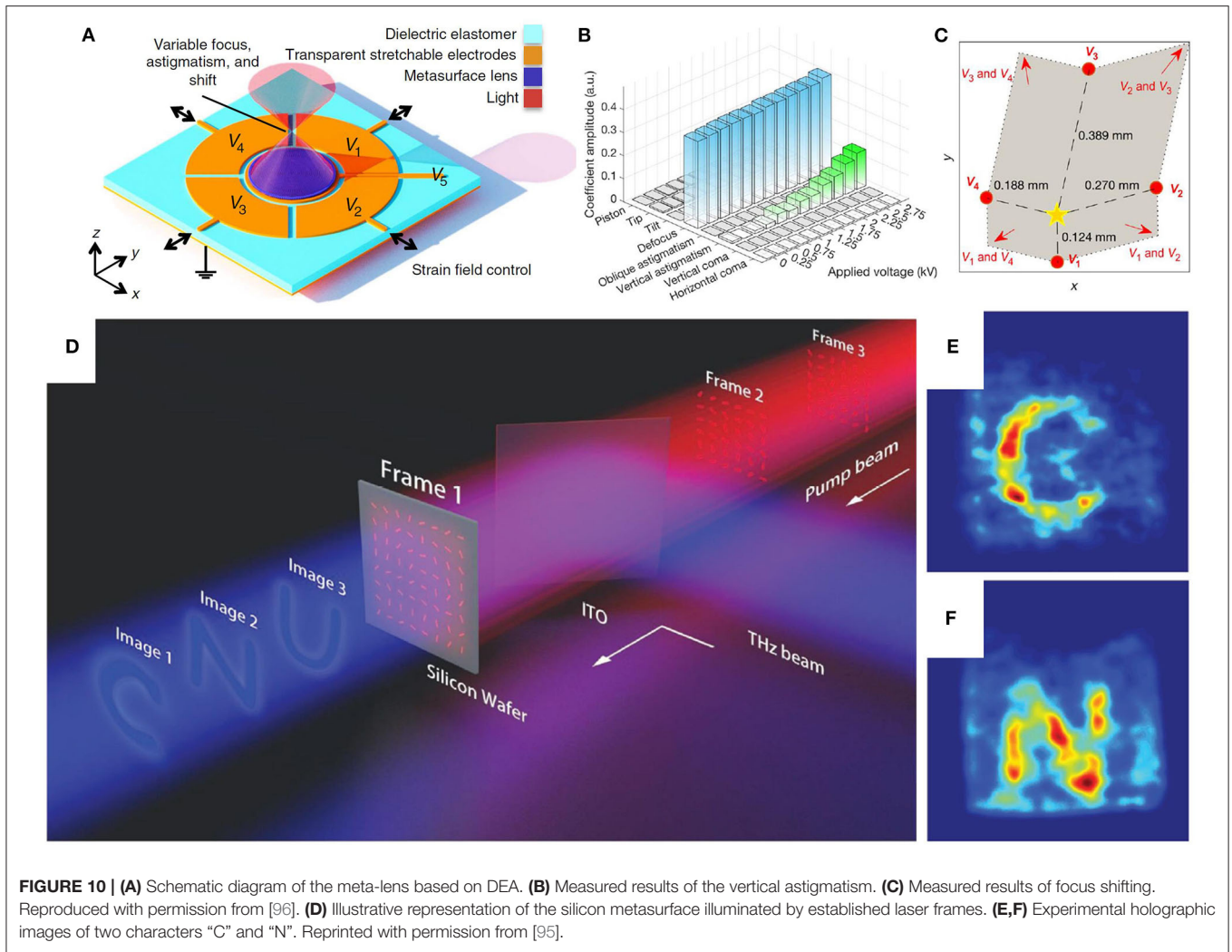
force, the meta-lens achieves adaptive profiles by electrically controlled artificial muscles that provide strain field. The schematic diagram of the meta-lens is illustrated in **Figure 10A**, in which a dielectric elastomer actuator (DEA) combined with five addressable electrodes is observed. After being attached to the middle electrode, the metasurface lens becomes stretchable under the strain field controlled by external voltages. To demonstrate the feasibility of the lens, the authors performed focus measurement and calculated Zernike coefficients of the phase profile as a demonstration of the vertical astigmatism. Measured results of focus shifting and the vertical astigmatism are respectively depicted in **Figures 10B,C**. For further verifying the mechanical robustness of the lens, the strain field was applied more than 1,000 cycles and no image degradation was observed. More recently, a novel photoexcited approach has been presented and applied to a thin silicon wafer for arbitrary terahertz wavefronts shaping [95], apart from the above electrically controllable metasurfaces. In such a work, inhomogeneity of the metasurface was caused by a local IMT in the silicon wafer, and Femtosecond laser was chosen as the photoexcitation. A conventional digital micromirror device (DMD) was employed to endow the incident laser pump with different

illumination patterns based on PB phase. Under an established laser frame, as shown in **Figure 10D**, those regions that are photoexcited can be regarded as a series of rod-shaped metal unit cells, and the unilluminated regions maintain the intrinsic insulator state. When laser pump is removed and re-modulated, the former frame can self-erase and another desirable frame can be excited. To demonstrate the photoexcited approach, the authors experimentally demonstrated the silicon metasurface to be a multifunctional one by implementing dynamic holographic imaging and focus shifting. Two characters “C” and “N” were imaged with clear outlines, as depicted in **Figures 10E,F**, and focus shifting was verified with focusing efficiency about 12%.

CODING AND PROGRAMMABLE METASURFACES FOR TERAHERTZ MANIPULATION

Coding Metasurfaces

Two concepts of digital characterization of metamaterial were proposed in the same year of 2014, but with essential differences. The concept of “digital metamaterials” [97], given



by Giovampaola and Engheta, contains definition of both “metamaterial bits” that characterizes two distinct permittivity functions and “metamaterial bytes” endowed by spatial mixture of metamaterial bits. Different from digital metamaterials that pertain to equivalent media theory, Cui et al. proposed the concept of “coding, digital, and programmable metamaterial” [98], which digitalizes phase responses instead of effective parameters. For example, phase responses 0 and π are correspondingly labeled as coding states “0” and “1” for a 1-bit situation. When the situation turns to 2-bit, four coding states “00,” “01,” “10,” and “11” correspond to phase responses 0, 0.5π , π , and 1.5π , respectively. Specifically, the refracted or reflected farfield function for an $N \times M$ coding metasurface illuminated by a normal incidence can be expressed as

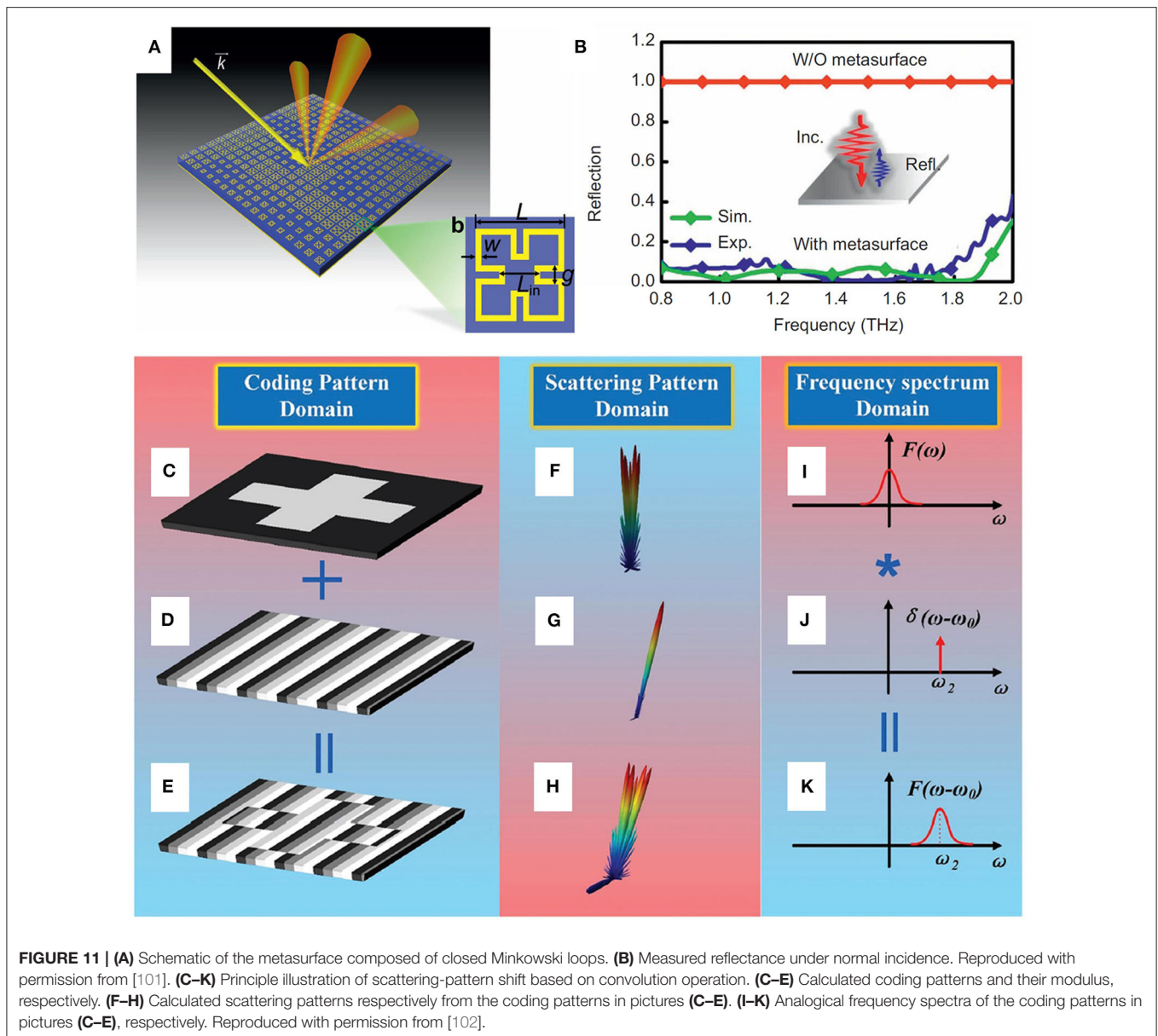
$$f(\theta, \varphi) = f_u(\theta, \varphi) \sum_{m=1}^N \sum_{n=1}^M \exp\{-i\{\varphi(m, n) + kP \sin \theta [(m - 0.5) \cos \varphi + (n - 0.5) \sin \varphi]\}\} \quad (3)$$

in which θ and φ are respectively the elevation angle and azimuth angle, k is the wavenumber, P is the dimension of the metasurface unit cell, and $f_u(\theta, \varphi)$ is the farfield function of each metasurface unit cell. Finally, the directivity can be represented as

$$D(\theta, \varphi) = 4\pi |f(\theta, \varphi)|^2 / \int_0^{2\pi} \int_0^{\pi/2} |f(\theta, \varphi)|^2 \sin \theta d\theta d\varphi \quad (4)$$

Compared with digital metamaterials, the coding concept is more suitable for simplifying the design of metasurfaces based on abrupt EM responses. More importantly, this concept plays a role in bridging the physical world and the digital world, making programmable metasurface a reality.

In the terahertz spectrum, the coding method has been employed to achieve untrammelled EM manipulations and simplify metasurface designs [99–105]. Regarding a ring-shaped unit cell as “1” element and a blank unit cell as “0” element, a 1-bit coding metasurface was constructed [100]. With a specific coding sequence, the authors demonstrated the coding metasurface with wave diffusion below -10 dB for both TE and TM incidences in a wide terahertz band from 0.8 to 1.4 THz; meantime, the incidence



insensitivity was confirmed up to 45° . In the same period, a novel coding unit cell etching closed Minkowski loop was proposed to design both 1-, 2-, and 3-bit coding metasurface based on geometry adjustment [101]. Finally, the authors experimentally verified a 2-bit coding metasurface with outstanding diffusion effect in wide bandwidth. A schematic of the metasurface is shown in **Figure 11A**, and the measured reflectance under normal incidence is recorded in **Figure 11B**, from which we can observe the reflected wave no more than 0.4 from 0.8 to 2 THz. Besides, the authors irradiated the sample at a large incidence angle to study the incidence insensitivity, and experimental results exhibit the metasurface with excellent diffusion along specular directions up to 40° . Later, Liu et al. proposed the principle of convolution operation on coding metasurface and provided an octagon-shaped unit cell to construct 2-bit

metasurface as verification [102]. Principle illustration of the scattering pattern shift based on the convolution operation is shown from **Figures 11C–K**. To testify the generality of the convolution principle, an arbitrary single-beam shifting function was performed on the 2-bit coding metasurface and got experimental demonstration. This work not only makes up the incomplete ability of the coding metasurface that only discrete angles can be manipulated but also provides a possibility for full-space beam control. Furthermore, coding metasurface can also be utilized to design multifunctional devices [104, 105]. As mentioned above, frequency multiplexing and polarization multiplexing are the two most commonly used methods to achieve function integration. In 2016, Liu et al. proposed a 2-bit anisotropic metasurface based on a dumbbell-shaped unit cell that can provide 2-bit phase states respectively under two

orthogonal linear polarizations [104]. Through endowing the metasurface with different coding sequences under orthogonal polarizations, dual functionality can be achieved. The authors demonstrated functional combination on one-fold metasurface, such as beam splitting and RCS reduction, beam deflection directing to disparate angles, and so on. In the same years, Liu et al. also verified a dual-functional metasurface based on frequency multiplexing [105]. Based on a double-layer I-shaped unit cell, 1-bit coding states can be obtained at 0.78 and 1.19 THz. Beam splitting pointing to different directions were measured to demonstrate the feasibility of frequency multiplexing of coding metasurfaces.

Programmable Metasurfaces

Programmable metasurface, as the active form of coding metasurface, requires flexible unit cells to realize state conversion in a real-time manner. By inputting pre-stored coding sequences, unit cells at specific locations exhibit local EM responses and a global EM response can be timely

generated for wave manipulations. In microwave frequencies, programmable metasurfaces have been widely studied and realized. The first microwave programmable metasurface was proposed by Cui et al. [98], and a field programmable gate array (FPGA) was introduced to provide different bias voltages through pins connected to each unit cell [98]. Several coding sequences were input to the FPGA, and output voltage sequences actuated conversion of EM responses, thus generating different scattering patterns. Thereafter, powerful programmable metasurfaces have been designed and contributed to different fields such as holography [106], imaging [107], space-time modulation [108], and communication system [109, 110], while in the terahertz spectrum, programmable metasurfaces are less studied, attributed to the difficulty not only in realizing tunability per unit cell but also in connecting sophisticated bias lines. In recent years, several theoretical analyses and simulation verifications of terahertz programmable metasurfaces have emerged as valuable attempts in this intriguing spectrum [111–114]. Without considering

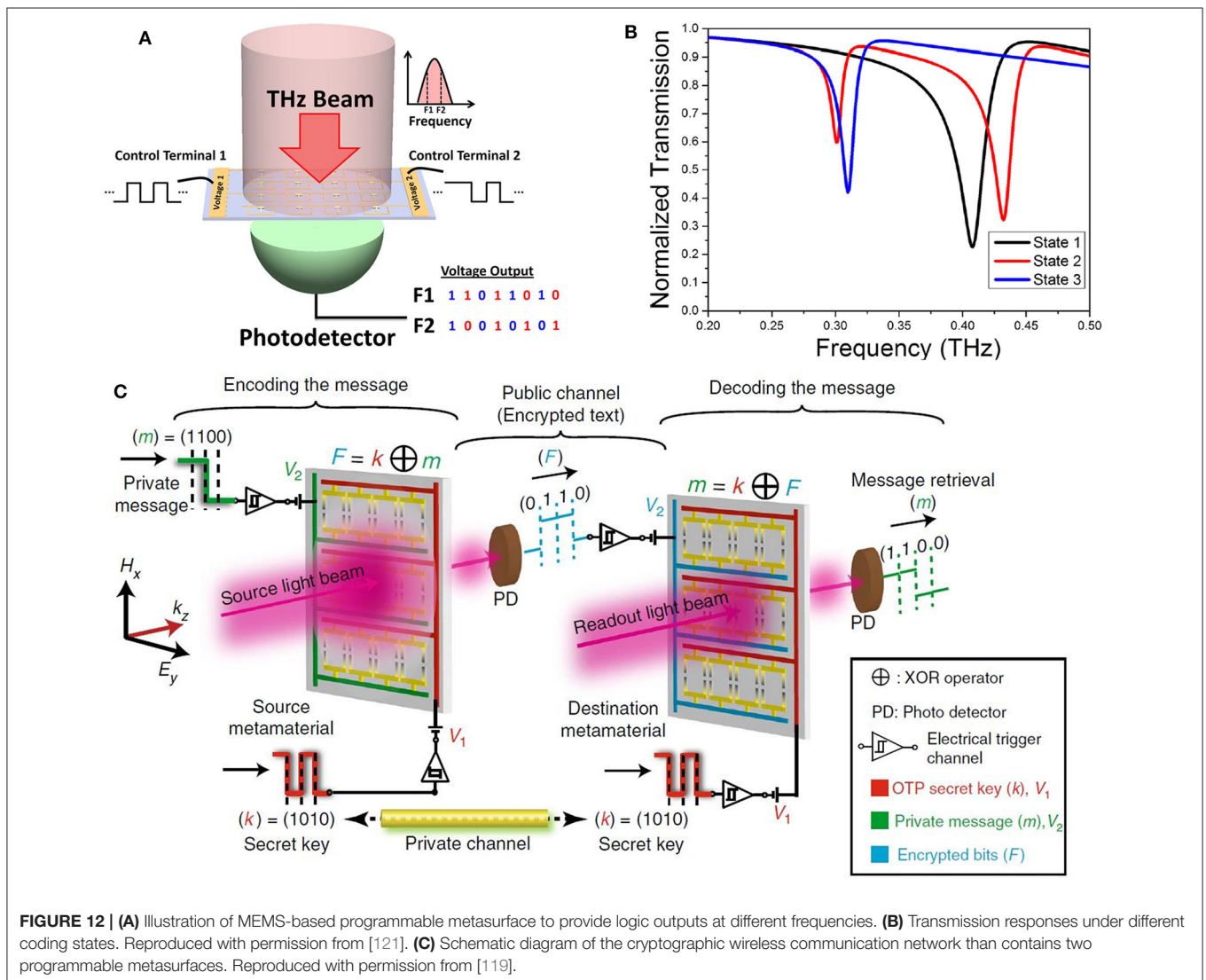
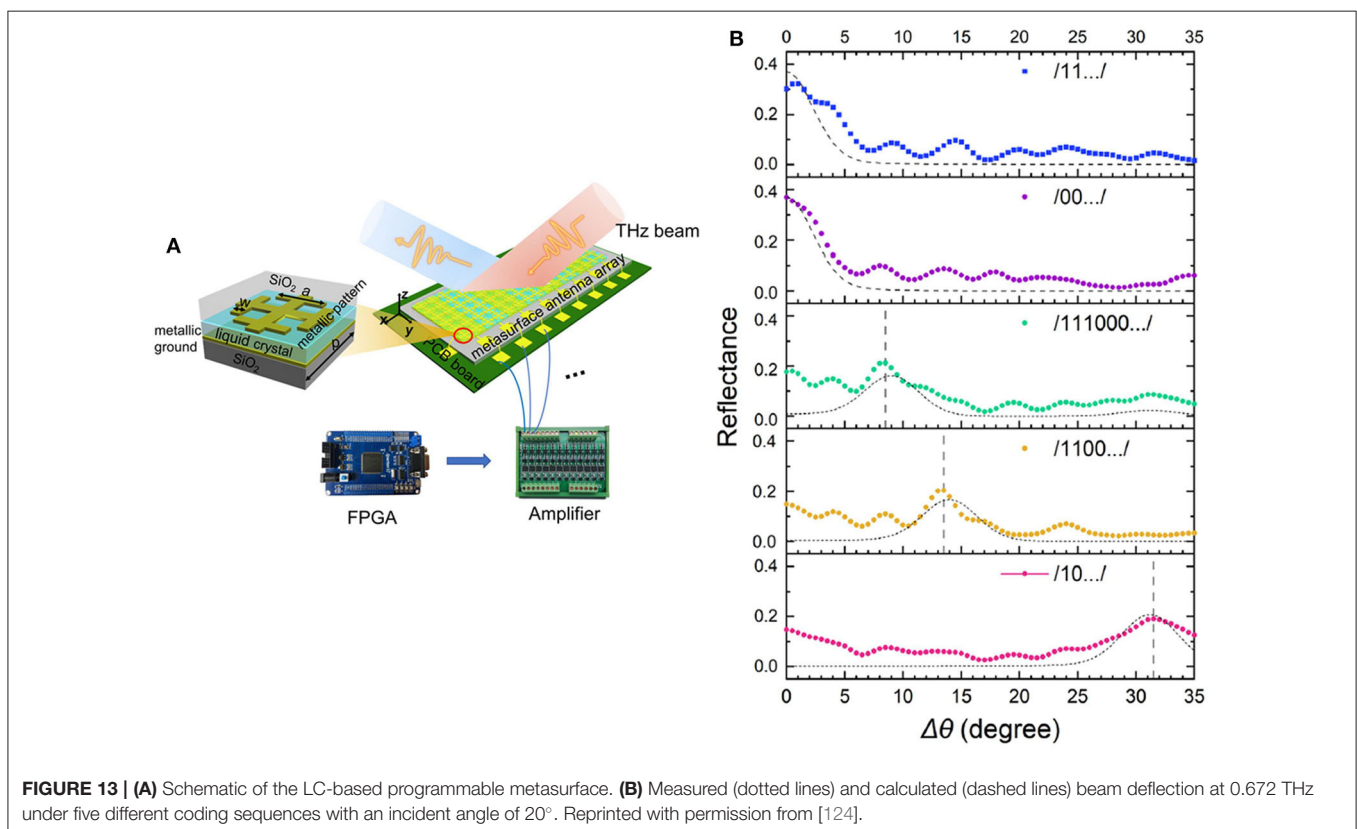


FIGURE 12 | (A) Illustration of MEMS-based programmable metasurface to provide logic outputs at different frequencies. **(B)** Transmission responses under different coding states. Reproduced with permission from [121]. **(C)** Schematic diagram of the cryptographic wireless communication network that contains two programmable metasurfaces. Reproduced with permission from [119].

sample fabrications as well as actual bias connections, programmable metasurfaces based on tunable components such as VO_2 , semiconductor germanium (Ge), and graphene have been proposed to demonstrate the feasibility of realizing real-time control and conversion of various functions. The attractive functions that have been implemented in the microwave band, like beam splitting and deflection [115], amplitude control [116], focus shifting [117], and space-time modulation [118], have also been theoretically and numerically verified for terahertz waves. However, theoretical analyses and simulations are not enough; only through practical measurements can terahertz programmable metasurface be proven with authenticity and practicability. To date, some experimental demonstrations have been presented and discussed [119–124].

For example, a MEMS-based programmable metasurface was proposed to perform different logical operations with frequency multiplexing [121]. By inputting pre-stored coding sequences to two bias terminals, as shown in **Figure 12A**, logical operations NOR and AND can be achieved. In the metasurface design, two SRR unit cells were considered as the effective unit cell; meantime, two bias terminals were connected to two SRRs separately to provide individual bias states. In this work, hanging of the bias was coded as “0,” and a pull-in voltage of 30 V was coded as “1.” Under different coding states “00,” “01/10,” and “11,” two resonances of transmission response can be obtained respectively at 0.26 and 0.36 THz,

as shown in **Figure 12B**. After defining the threshold of the transmission amplitude, NOR and AND operations were realized at the two frequency points. After that, Manjappa et al. proposed a programmable Fano resonant metasurface and experimentally verified it with multiple input–output (MIO) states [119]. By biasing two SRR structures unequally to increase and decrease the asymmetry δ , Fano resonance can be tuned actively and one can define different input–output states and then utilize them for various applications. Based on the realized programmable metasurface, the authors performed multiple wave-based logic operations at terahertz frequencies. Two metastable states defined by two bias inputs 0 and 35 V are represented by binary codes. The “up-state” of the metasurface is defined as binary “0,” and the “down-state” corresponds to “1.” Under different digital codes, logical operations such as XOR, XNOR, PASS, and NOT logic gates in the far-field optical states were demonstrated using the single metasurface platform. It is noted that the XOR functionality possesses a unique property of pseudorandom generation and can serve as a key component of encryption/decryption techniques for communication systems. As depicted in **Figure 12C**, a cryptographic wireless communication network containing two programmable metasurfaces has been proposed. It is obvious that private messages can be encrypted by secret keys after passing through the source metasurface, and the destination metasurface can retrieve original messages. More recently, Cong et al. proposed a kind of MEMS-based programmable metasurface



relying on chiral transformations [120]. Except for performing logical operations like XOR and OR, the presented metasurface can be used to perform multiplexed intensity modulation because of its high-intensity extinction ratio at two frequencies. With the aid of a wire-grid polarizer (WGP), two complementary images can be respectively obtained at 0.4 and 0.7 THz under orthogonal polarizations. The metasurface can transmit abundant and multiplexed information in a real-time manner, which provides potentials in increasing communication capacities. Apart from logical operations, terahertz programmable metasurfaces have also been employed to realize other functions, such as anisotropic switching and beam steering [122–124]. For instance, Pitchappa et al. proposed a type of metasurface structure with particular capability in switching terahertz anisotropy [122]. The metasurface unit cell was composed of four cantilevers with a cross-shaped arrangement. Two bond pads (named MCX and MCY) were introduced to power the cantilevers in x and y directions separately. By encoding MCX and MCY with either “ON” or “OFF” states, different transmission amplitudes can be achieved owing to the structure anisotropy. Finally, a noticeable anisotropy switching with a difference of 1.8 is measured. More recently, Wu et al. proposed an LC-based 1-bit programmable metasurface to achieve beam steering [124]. A Jerusalem cross was chosen as the upper pattern with LCs embedded below as the substrate. An FPGA and an amplifier array were integrated to provide two bias voltages 0 and 40 V, which are coded as “0” and “1,” respectively. The schematic of the LC-based programmable metasurface is shown in **Figure 13A**. Then, by actuating different coding sequences to the metasurface, different reflection angles can be steered in

real time. Measured results are depicted in **Figure 13B**, where simulation results are also provided as reference. It is obvious that both simulated and measured results demonstrate a desired beam steering effect.

SUMMARY

As an artificial structure, metasurface exhibits unprecedented capabilities in manipulating wave characteristics, in the microwave, terahertz, and optical frequency bands [125–127]. In this article, we introduced the development of metasurface and emphasis on recent advances in the terahertz spectrum. Terahertz passive metasurfaces, terahertz active metasurfaces, terahertz coding metasurfaces, and terahertz programmable metasurfaces are within our retrospection.

First of all, passive metasurfaces with fascinating functions, especially those with multifunctional properties, are briefly reviewed. Multifunctional characteristic can be acquired by two means, one is frequency multiplexing and the other is polarization multiplexing. Extensive researches on versatility plays an extremely important role in improving device integration. Thereafter, several achievements on active metasurfaces integrated with tunable materials or advanced technics, such as semiconductor, VO_2 , LC, TCO, graphene, 2DEG, elastomer, perovskite, quantum dot, superconductor, and MEMS, are concisely looked back. Although passive metasurfaces have exhibited high freedom in regulating multiple functions, fixed prototypes make adjustability improbable and limit metasurfaces to restricted scenarios, while active

TABLE 1 | Comparison of several terahertz metasurfaces, including passive metasurfaces, active metasurfaces, coding metasurfaces, and programmable metasurfaces.

Types	Methods or technologies	Operating frequencies	Functions and applications	References
Monofunctional passive metasurfaces	Deep subwavelength structure	0.88 THz	Beam deflection	[19]
Frequency multiplexing metasurfaces	PB phase	0.5 & 0.63 THz	Holography	[31]
	PB phase	0.4 & 0.85 THz	Beam deflection	[32]
Polarization multiplexing metasurfaces	PB phase	0.6 & 0.8 THz	Holography	[35]
	PB phase	0.65–0.95 THz	Focusing	[36]
Active metasurfaces with functional tunability	Anisotropy	1 THz	OAM & bessel beam	[38]
	Superconductor	0.341 THz	Transmittance modulation	[66]
	Perovskite	0.86 THz/1.12 THz	Transmittance modulation	[69]
	Quantum dot	0.5 THz	Transmittance modulation	[73]
Active metasurfaces with dynamically functional multiplexing	Graphene	5 THz	Focus tuning	[80]
	VO_2	0.63 & 0.864 THz	Electrical switching & rewritable memory & ultrafast modulation	[94]
Coding metasurfaces	Semiconductor (sili con)	0.5 THz	Reconfigurable holography	[95]
	1-bit coding method	0.8–1.4 THz	Wave diffusion	[100]
Programmable metasurfaces	2-bit Coding method & anisotropy	0.9–1.5 THz	Beam splitting & RCS reduction	[104]
	MEMS	0.56 THz	Logic operations (XOR, XNOR, PASS & NOT)	[119]
	Liquid crystal	0.672 THz	Beam Steering	[124]
	MEMS	0.4 & 0.7 THz	Logic operations & multiplexed intensity modulation	[120]

metasurfaces can get rid of this limitation and widen application scopes. In particular, those metasurfaces with dynamically functional multiplexing can offer multifunctional choices in excess of tunability, thus providing the possibility for coexistence of advanced performance and high integration. Finally, some outcomes of coding metasurfaces and programmable metasurfaces are simply retrospect. Characterized by digital bits, coding metasurfaces bond physical EM responses and digital signals without intermediary [128, 129]. Programmable metasurface, as an active evolution of coding metasurface, not only can perform information processing but also can realize desired EM modulation. Therefore, programmable metasurfaces can serve as an efficient and highly integrated approach for terahertz radar, real-time imaging, and communication system [130]. For intuitive overview, comparisons of several aforementioned terahertz metasurfaces are listed in **Table 1**.

In summary, multifunctional metasurfaces and programmable metasurfaces play important roles in device integration and information handling, particularly at the

fascinating terahertz band. Based on these listed advances, we prospect and highlight a further trend of developing terahertz multifunctional metasurfaces and programmable metasurfaces, which we believe will make unprecedented contributions to the terahertz field.

AUTHOR CONTRIBUTIONS

All authors listed have made a substantial, direct and intellectual contribution to the work, and approved it for publication.

FUNDING

This work was supported in part from the Foundation of National Key Research and Development Program of China under Grant Nos. 2017YFA0700201, 2017YFA0700202, and 2016YFC0800401; National Ten-Thousands Talents Plan; National Excellent Doctoral Dissertation of China under Grant No. 201444; the National Science Foundation of China under Grant Nos. 61890540, 61890544, and 61890545.

REFERENCES

- Phillips TG, Keene J. Submillimeter astronomy. *Proc IEEE*. (1992) **80**:1662–78. doi: 10.1109/5.175248
- He JW, Dong T, Chi BH, Zhang Y. Metasurfaces for terahertz wavefront modulation: a review. *J Infrared Millim Terahertz Waves*. (2020) **41**:607–31. doi: 10.1007/s10762-020-00677-3
- Wang L, Zhang YX, Guo XQ, Chen T, Liang HJ, Hao XL, et al. A review of THz modulators with dynamic tunable metasurfaces. *Nanomaterials*. (2019) **9**:965. doi: 10.3390/nano9070965
- Gospodaric J, Kuzmenko A, Pimenov A, Huber C, Suess D, Rotter S, et al. 3D-printed phase waveplates for THz beam shaping. *Appl Phys Lett*. (2018) **112**:221104. doi: 10.1063/1.5027179
- Scherger B, Born N, Jansen C, Schumann S, Koch M, Wiesauer K. Compression molded terahertz transmission blaze-grating. *IEEE Trans Terahertz Sci Technol*. (2012) **2**:556–61. doi: 10.1109/TTHZ.2012.2210892
- Minkevicius L, Indrisiunas S, Sniakaus R, Voisiat B, Janonis V, Tamosiunas V, et al. Terahertz multilevel phase fresnel lenses fabricated by laser patterning of silicon. *Opt Lett*. (2017) **42**:1875–78. doi: 10.1364/OL.42.001875
- Smith DR, Schultz S, Markos P, Soukoulis CM. Determination of effective permittivity and permeability of metamaterials from reflection and transmission coefficients. *Phys Rev B*. (2001) **65**:195104. doi: 10.1103/PhysRevB.65.195104
- Kuester EF, Mohamed MA, Piket-May M, Holloway CL. Averaged transition conditions for electromagnetic fields at a metafilm. *IEEE Trans Antennas Propag*. (2003) **51**:2641–51. doi: 10.1109/TAP.2003.817560
- Yu NF, Genevet P, Kats MA, Aieta F, Tetienne JP, Capasso F, et al. Light propagation with phase discontinuities: generalized laws of reflection and refraction. *Science*. (2011) **334**:333. doi: 10.1126/science.1210713
- Pfeiffer C, Grbic A. Metamaterial Huygens' surfaces: tailoring wave fronts with reflectionless sheets. *Phys Rev Lett*. (2013) **110**:197401. doi: 10.1103/PhysRevLett.110.197401
- Paniagua-Dominguez R, Yu YF, Miroshnichenko AE, Krivitsky LA, Fu YH, Valuckas V, et al. Generalized brewster effect in dielectric metasurfaces. *Nat Commun*. (2016) **7**:10362. doi: 10.1038/ncomms10362
- Huang H, Shen ZX. Brewster lens with perfect wave refraction. *IEEE Trans Antennas Propag*. (2020) **68**:6204–13. doi: 10.1109/TAP.2020.2990232
- Tian HW, Jiang WX, Li X, Zhang XG, Yang ZY, Cui TJ. Generation of high-order orbital angular momentum beams and split beams simultaneously by employing anisotropic coding metasurfaces. *J Opt*. (2019) **21**:065103. doi: 10.1088/2040-8986/ab16b9
- Zhao J, Cheng Q, Wang XK, Yuan MJ, Zhou X, Fu, et al. J. et al. Controlling the bandwidth of terahertz low-scattering metasurfaces. *Adv Optical Mater*. (2016) **4**:1773–9. doi: 10.1002/adom.201600202
- Sun QS, He YZ, Liu K, Fan ST, Parrott EPJ, Pickwell-MacPherson E. Recent advances in terahertz technology for biomedical applications. *Quant Imaging Med Surg*. (2017) **7**:345–55. doi: 10.21037/qims.2017.06.02
- True AB, Schroeck K, French TA, Schmuttenmaer CA. Terahertz spectroscopy of histidine enantiomers and polymorphs. *J Infrared Milli Terahz Waves*. (2011) **32**:691–8. doi: 10.1007/s10762-010-9645-9
- Liu LX, Zhang XQ, Kenney M, Su XQ, Xu NN, Ouyang CM, et al. Broadband metasurfaces with simultaneous control of phase and amplitude. *Adv Mater*. (2014) **26**:5031–6. doi: 10.1002/adma.201401484
- Zhang XQ, Zhang X, Tian Z, Yue W, Gu J, Zhang S, et al. Broadband terahertz wave deflection based on C-shape complex metamaterials with phase discontinuities. *Adv Mater*. (2013) **25**:4567–72. doi: 10.1002/adma.201204850
- Liu MK, Yang QL, Rifat AA, Raj V, Komar A, Han JG, et al. Deeply subwavelength metasurface resonators for terahertz wavefront manipulation. *Adv Optical Mater*. (2019) **7**:21. doi: 10.1002/adom.201900736
- Zhao H, Quan BG, Wang XK, Gu CZ, Li JJ, Zhang Y. Demonstration of orbital angular momentum multiplexing and demultiplexing based on a metasurface in the terahertz band. *ACS Photonics*. (2018) **5**:1726–32. doi: 10.1021/acsp Photonics.7b01149
- Jia M, Wang Z, Li HT, Wang XK, Luo WJ, Sun SL, et al. Efficient manipulations of circularly polarized terahertz waves with transmissive metasurfaces. *Light Sci Appl*. (2019) **8**:16. doi: 10.1038/s41377-019-0127-0
- Guo JY, Wang XK, He JW, Zhao H, Feng SF, Han P, et al. Generation of radial polarized Lorentz beam with single layer metasurface. *Adv Opt Mater*. (2017) **6**:1700925. doi: 10.1002/adom.201700925
- Chen PY, Soric J, Padooru YR, Bernety HM, Yakovlev AB, Alu A. Nanostructured graphene metasurface for tunable terahertz cloaking. *New J Phys*. (2013) **15**:123029. doi: 10.1088/1367-2630/15/12/123029
- He JW, Ye JS, Wang SK, Kan Q, Zhang Y. A broadband terahertz ultrathin multi-focus lens. *Sci Rep*. (2016) **6**:28800. doi: 10.1038/srep28800
- Yi H, Qu SW, Chen BJ, Bai X, Ng KB, Chan CH. Flat terahertz reflective focusing metasurface with scanning ability. *Sci Rep*. (2017) **7**:3478. doi: 10.1038/s41598-017-03752-3

26. Liu LM, Zarate Y, Hattori HT, Neshev DN, Shadrivov LV, Powell DA. Terahertz focusing of multiple wavelengths by graphene metasurfaces. *Appl Phys Lett*. (2016) **108**:031106. doi: 10.1063/1.4940231
27. Mou NL, Sun SL, Dong HX, Dong SH, He Q, Zhou L, et al. Hybridization-induced broadband terahertz wave absorption with graphene metasurfaces. *Opt Express*. (2018) **26**:11728. doi: 10.1364/OE.26.011728
28. Cong LQ, Xu NN, Han JG, Zhang WL, Singh R. Tunable dispersion-free terahertz metadvice with Pancharatnam–Berry-phase-enabled modulation and polarization control. *Adv Mater*. (2015) **27**:6630–6. doi: 10.1002/adma.201502716
29. Cong LQ, Xu NN, Zhang WL, Singh R. Polarization control in terahertz metasurfaces with the lowest order rotational symmetry. *Adv Optical Mater*. (2015) **3**:1176–83. doi: 10.1002/adom.201500100
30. Grady NK, Heyes JE, Chowdhury DR, Zeng Y, Reiten MT, Azad AK, et al. Terahertz metamaterials for linear polarization conversion and anomalous refraction. *Science*. (2013) **340**:1304–7. doi: 10.1126/science.1235399
31. Wang B, Quan BG, He JW, Xie ZW, Wang XK, Li JJ, et al. Wavelength de-multiplexing metasurface hologram. *Sci Rep*. (2016) **6**:35657. doi: 10.1038/srep35657
32. Wang X, Ding J, Zheng BW, An SS, Zhai GH, Zhang HL. Simultaneous realization of anomalous reflection and transmission at two frequencies using bi-functional metasurfaces. *Sci Rep*. (2018) **8**:1876. doi: 10.1038/s41598-018-20315-2
33. Zi JC, Li YF, Feng X, Xu Q, Liu HC, Zhang XX, et al. Dual-functional terahertz waveplate based on all-dielectric metamaterial. *Phys Rev Appl*. (2020) **13**:034042. doi: 10.1103/PhysRevApplied.13.034042
34. Zhang XF, Gong HH, Li Z, Xie JY, Cheng QQ, Chen L, et al. Metasurface for multi-channel terahertz beam splitters and polarization rotators. *Appl Phys Lett*. (2018) **112**:171111. doi: 10.1063/1.5028401
35. Wang Q, Zhang XQ, Plum E, Xu Q, Wei MG, Xu YH, et al. Polarization and frequency multiplexed terahertz meta-holography. *Adv Optical Mater*. (2017) **5**:1700277. doi: 10.1002/adom.201700277
36. Wang S, Wang XK, Kan Q, Ye JS, Feng SF, Sun WF, et al. Spin-selected focusing and imaging based on metasurface lens. *Opt Express*. (2015) **23**:26434–41. doi: 10.1364/OE.23.026434
37. Li JQ, Zhang L, Zhang M, Su H, Li IL, Ruan SC, et al. Wearable conformal metasurfaces for polarization division multiplexing. *Adv Optical Mater*. (2020) **8**:2000068. doi: 10.1002/adom.202000068
38. Zhang HF, Zhang XQ, Xu Q, Tian CX, Wang Q, Xu YH, et al. High-efficiency dielectric metasurfaces for polarization dependent terahertz wavefront manipulation. *Adv Optical Mater*. (2017) **6**:1700773. doi: 10.1002/adom.201700773
39. Isic G, Sinatkas G, Zografopoulos DC, Vasic B, Ferraro A, Beccherelli R, et al. Electrically tunable metal–semiconductor–metal terahertz metasurface modulators. *IEEE J Sel Top Quantum Electron*. (2019) **25**:8500 108. doi: 10.1109/JSTQE.2019.2893762
40. Zhou GC, Dai PH, Wu JB, Jin BB, Wen QY, Zhu GH, et al. Broadband and high modulation-depth THz modulator using low bias controlled VO₂integrated metasurface. *Opt Express*. (2017) **25**:17322–8. doi: 10.1364/OE.25.017322
41. Shen ZX, Zhou SH, Ge SJ, Duan W, Ma LL, Lu YQ, et al. Liquid crystal tunable terahertz lens with spin-selected focusing property. *Opt Express*. (2019) **27**:8800–7. doi: 10.1364/OE.27.008800
42. Huang YW, Lee HWH, Sokhoyan R, Pala RA, Thyagarajan K, Han S, et al. Gate-tunable conducting oxide metasurfaces. *Nano Lett*. (2016) **16**:5319–25. doi: 10.1021/acs.nanolett.6b00555
43. Scalari G, Maissen C, Turcinková D, Hagenmüller D, De Liberato S, Ciuti, et al. Ultrastrong coupling of the cyclotron transition of a 2D electron Gas to a THz metamaterial. *Science*. (2012) **335**:1323–6. doi: 10.1126/science.1216022
44. Chanana A, Liu XJ, Zhang C, Vardeny ZV, Nahata A. Ultrafast frequency-agile terahertz devices using methylammonium lead halide perovskites. *Sci Adv*. (2018) **4**:ear7353. doi: 10.1126/sciadv.aar7353
45. Yang Y, Li JN, Li J, Huang J, Li QY, Zhang YT, et al. Optical control of terahertz plasmon-induced transparency based on hybrid CsPbBr₃ quantum dot metasurfaces. *Opt Express*. (2020) **28**:24047–55. doi: 10.1364/OE.399822
46. Savinov V, Tsiatmas A, Buckingham AR, Fedotov VA, de Groot PAJ, Zheludev NI. Flux exclusion superconducting quantum metamaterial: towards quantum-level switching. *Sci Rep*. (2012) **2**:450. doi: 10.1038/srep00450
47. Schalch JS, Post K, Duan GW, Zhao XG, Kim YD, Hone J, et al. Strong metasurface-josephson plasma resonance coupling in superconducting La₂-xSrxCuO₄. *Adv Optical Mater*. (2019) **7**:1900712. doi: 10.1002/adom.201900712
48. He Q, Sun L, Zhou L. Tunable/reconfigurable metasurfaces: physics and applications. *Research*. (2019) **2019**:1–6. doi: 10.34133/2019/1849272
49. Savo S, Shrekenhamer D, Padilla WJ. Liquid crystal metamaterial absorber spatial light modulator for THz applications. *Adv Optical Mater*. (2014) **2**:275–9. doi: 10.1002/adom.201300384
50. Li Q, Gupta M, Zhang XQ, Wang S, Chen T, Singh R, et al. Active control of asymmetric fano resonances with graphene–silicon-integrated terahertz metamaterials. *Adv Mater Technol*. (2020) **5**:1900840. doi: 10.1002/admt.201900840
51. Shih K, Pitchappa P, Manjappa M, Ho CP, Singh R, Yang B, et al. Active MEMS metamaterials for THz bandwidth control. *Appl Phys Lett*. (2017) **110**:161108. doi: 10.1063/1.4980115
52. Manjappa M, Srivastava YK, Cong LQ, Al-Naib I, Singh R. Active photoswitching of sharp fano resonances in THz metadvice. *Adv Mater*. (2016) **29**:1603355. doi: 10.1002/adma.201603355
53. Kim TT, Kim H, Kenney M, Park HS, Kim HD, Min B, et al. Amplitude modulation of anomalously refracted terahertz waves with gated-graphene metasurfaces. *Adv Optical Mater*. (2017) **6**:1700507. doi: 10.1002/adom.201700507
54. Deng LY, Teng JH, Liu HW, Wu QY, Tang J, Zhang XH, et al. Direct optical tuning of the terahertz plasmonic response of InSb subwavelength gratings. *Adv Optical Mater*. (2013) **1**:128–32. doi: 10.1002/adom.201200032
55. Buchnev O, Podoliak N, Kaczmarek M, Zheludev NI, Fedotov VA. Electrically controlled nanostructured metasurface loaded with liquid crystal: toward multifunctional photonic switch. *Adv Optical Mater*. (2014) **3**:674–9. doi: 10.1002/adom.201400494
56. Chen HT, O'Hara JF, Azad AK, Taylor AJ, Averitt RD, Shrekenhamer DB, et al. Experimental demonstration of frequency-agile terahertz metamaterials. *Nat Photon*. (2008) **2**:295–8. doi: 10.1038/nphoton.2008.52
57. Shrekenhamer D, Montoya J, Krishna S, Padilla WJ. Four-color metamaterial absorber THz spatial light modulator. *Adv Optical Mater*. (2013) **1**:905–9. doi: 10.1002/adom.201300265
58. Valmorra F, Scalari G, Maissen C, Fu WY, Schönenberger C, Choi JW, et al. Low-bias active control of terahertz waves by coupling large-area CVD graphene to a terahertz metamaterial. *Nano Lett*. (2013) **13**:3193–8. doi: 10.1021/nl4012547
59. DeglInnocenti R, Jessop DS, Shah YD, Sibik J, Zeitler JA, Kidambi PR, et al. Low-bias terahertz amplitude modulator based on split-ring resonators and graphene. *ACS Nano*. (2014) **8**:2548–54. doi: 10.1021/nl406136c
60. Liu MK, Hwang HY, Tao H, Strikwerda AC, Fan KB, Keiser GR, et al. Terahertz-field-induced insulator-to-metal transition in vanadium dioxide metamaterial. *Nature*. (2012) **487**:345–8. doi: 10.1038/nature11231
61. Ding L, Luo XS, Cheng L, Thway M, Song JF, Chua SJ, et al. Electrically and thermally tunable smooth silicon metasurfaces for broadband terahertz antireflection. *Adv Optical Mater*. (2018) **6**:1800928. doi: 10.1002/adom.201800928
62. Zhang YX, Qiao S, Liang SX, Wu ZH, Yang ZQ, Feng ZH, et al. Gbps terahertz external modulator based on a composite metamaterial with a double-channel heterostructure. *Nano Lett*. (2015) **15**:3501–6. doi: 10.1021/acs.nanolett.5b00869
63. Lee SH, Choi M, Kim TT, Lee S, Liu M, Yin XB, et al. Switching terahertz waves with gate-controlled active graphene metamaterials. *Nat Mater*. (2012) **11**:936–41. doi: 10.1038/nmat3433
64. Chen HT, Padilla J, Cich MJ, Azad AK, Averitt RD, Taylor, et al. J. A metamaterial solid-state terahertz phase modulator. *Nat Photon*. (2009) **3**:148–51. doi: 10.1038/nphoton.2009.3
65. Miao ZQ, Wu Q, Li X, He Q, Ding K, An ZH, et al. Widely tunable terahertz phase modulation with Gate-controlled graphene metasurfaces. *Phys Rev X*. (2015) **5**:041027. doi: 10.1103/PhysRevX.5.041027

66. Li C, Wu JB, Jiang SL, Su RF, Zhang CH, Jiang CT, et al. Electrical dynamic modulation of THz radiation based on superconducting metamaterials. *Appl Phys Lett*. (2017) **111**:092601. doi: 10.1063/1.4997097
67. Cao W, Singh R, Zhang CH, Han JG, Tonouchi M, Zhang WL. Plasmon-induced transparency in metamaterials: active near field coupling between bright superconducting and dark metallic mode resonators. *Appl Phys Lett*. (2013) **103**:101106. doi: 10.1063/1.4819389
68. Scalari G, Maissen C, Cibella S, Leoni R, Faist J. High quality factor, fully switchable terahertz superconducting metasurface. *Appl Phys Lett*. (2014) **105**:261104. doi: 10.1063/1.4905199
69. Zhou JH, Hu YZ, Jiang T, Ouyang H, Li H, Sui YZ, et al. Ultrasensitive polarization-dependent terahertz modulation in hybrid perovskites plasmon-induced transparency devices. *Photon Res*. (2019) **7**:994–1002. doi: 10.1364/PRJ.7.000994
70. Chanana A, Zhai YX, Baniya S, Zhang C, Vardeny ZV, Nahata A. Colour selective control of terahertz radiation using two-dimensional hybrid organic inorganic lead-trihalide perovskites. *Nat Commun*. (2017) **8**:1328. doi: 10.1038/s41467-017-01517-0
71. Manjappa M, Srivastava YK, Solanki A, Kumar A, Sum TC, Singh R. Hybrid lead halide perovskites for ultrasensitive photoactive switching in terahertz metamaterial devices. *Adv Mater*. (2017) **29**:1605881. doi: 10.1002/adma.201605881
72. Cong L, Srivastava YK, Solanki A, Sum TC, Singh R. Perovskite as a platform for active flexible metaphotonic devices. *ACS Photon*. (2017) **4**:1595–601. doi: 10.1021/acsp Photonics.7b00191
73. Xiong RH, Peng XQ, Li JS. Terahertz switch utilizing inorganic perovskite-embedded metasurface. *Front Phys*. (2020) **8**:141. doi: 10.3389/fphy.2020.00141
74. Wang X, Li YY, Toufanian R, Kogos LC, Dennis AM, Paiella R. Geometrically tunable beamed light emission from a quantum-dot ensemble near a gradient metasurface. *Adv Optical Mater*. (2020) **8**:1901951. doi: 10.1002/adom.201901951
75. Yakimov AI, Kirienko VV, Armbrister VA, Bloshkin AA, Dvurechenskii AV. Surface Plasmon dispersion in a mid-infrared Ge/Si quantum dot photodetector coupled with a perforated gold metasurface. *Appl Phys Lett*. (2018) **112**:171107. doi: 10.1063/1.5029289
76. Zhang CH, Zhou GC, Wu JB, Tang YH, Wen QY, Li SX, et al. Active control of terahertz waves using vanadium-dioxide-embedded metamaterials. *Phys Rev Appl*. (2019) **11**:054016. doi: 10.1103/PhysRevApplied.11.054016
77. Roy T, Zhang SY, Jung II W, Troccoli M, Capasso F, Lopez D. Dynamic metasurface lens based on MEMS technology. *APL Photon*. (2017) **3**:021302. doi: 10.1063/1.5018865
78. Huang ZD, Hu B, Liu WG, Liu J, Wang YT. Dynamical tuning of terahertz meta-lens assisted by graphene. *J Opt Soc Am B*. (2017) **34**:1848–54. doi: 10.1364/JOSAB.34.001848
79. Liu WG, Hu B, Huang ZD, Guan HY, Li HT, Wang XK. Graphene-enabled electrically controlled terahertz meta-lens. *Photon Res*. (2018) **6**:703–8. doi: 10.1364/PRJ.6.000703
80. Ding P, Li Y, Shao L, Tian XM, Wang JQ, Fan CZ. Graphene aperture-based metalens for dynamic focusing of terahertz waves. *Opt Express*. (2018) **26**:28038–50. doi: 10.1364/OE.26.028038
81. Chen XY, Tian Z, Lu YC, Xu YH, Zhang XQ, Ouyang CM, et al. Electrically tunable perfect terahertz absorber based on a graphene salisbury screen hybrid metasurface. *Adv Opt. Mater*. (2019) **8**:1900660. doi: 10.1002/adom.201900660
82. Sadat ES, Fallahi A, Yahaghi A. Evolutionary optimization of graphene-metal metasurfaces for tunable broadband terahertz absorption. *IEEE Trans Antennas Propag*. (2017) **65**:1464–7. doi: 10.1109/TAP.2016.2647580
83. Yang YM, Kamaraju N, Campione S, Liu S, Reno JL, Sinclair MB, et al. Transient GaAs plasmonic metasurfaces at terahertz frequencies. *ACS Photon*. (2016) **4**:15–21. doi: 10.1021/acsp Photonics.6b00735
84. Chu CH, Tseng ML, Chen J, Wu PC, Chen YH, Wang HC, et al. Active dielectric metasurface based on phase-change medium. *Laser Photon Rev*. (2016) **10**:986–94. doi: 10.1002/lpor.201600106
85. Su XQ, Ouyang CM, Xu NN, Cao W, Wei X, Song GF, et al. Active metasurface terahertz deflector with phase discontinuities. *Opt Express*. (2015) **23**:27152–8. doi: 10.1364/oe.23.027152
86. Hashemi MRM, Yang SH, Wang TY, Sepúlveda N, Jarrahi M. Electronically-controlled beam-steering through vanadium dioxide metasurfaces. *Sci Rep*. (2016) **6**:35439. doi: 10.1038/srep35439
87. Vasic B, Isic G, Beccherelli R, Zografopoulos DC. Tunable beam steering at terahertz frequencies using reconfigurable metasurfaces coupled with liquid crystals. *IEEE J Sel Top Quantum Electron*. (2020) **26**:1–9. doi: 10.1109/JSTQE.2019.2956856
88. Zhao XG, Schalch J, Zhang JG, Seren HR, Duan GW, Averitt RD, et al. Electromechanically tunable metasurface transmission waveplate at terahertz frequencies. *Optica*. (2018) **5**:303–10. doi: 10.1364/optica.5.000303
89. Nakata Y, Fukawa K, Nakanishi T, Urade Y, Okimura K, Miyamaru F. Reconfigurable terahertz quarter-wave plate for helicity switching based on babinet inversion of an anisotropic checkerboard metasurface. *Phys Rev Appl*. (2019) **11**:044008. doi: 10.1103/PhysRevApplied.11.044008
90. Watt CM, Shrekenhamer D, Montoya J, Lipworth G, Hunt J, Sleasman T, et al. Terahertz compressive imaging with metamaterial spatial light modulators. *Nat Photon*. (2014) **8**:605–9. doi: 10.1038/nphoton.2014.139
91. Cong LQ, Pitchappa P, Wu Y, Ke L, Lee CK, et al. Active multifunctional microelectromechanical system metadevices: applications in polarization control, wavefront deflection, and holograms. *Adv Optical Mater*. (2016) **5**:1600716. doi: 10.1002/adom.201600716
92. Cong LQ, Srivastava YK, Zhang HF, Zhang XQ, Han JG, Singh R. All-optical active THz metasurfaces for ultrafast polarization switching and dynamic beam splitting. *Light Sci Appl*. (2018) **7**:1–9. doi: 10.1038/s41377-018-0024-y
93. Liu L, Kang L, Mayer TS, Werner DH. Hybrid metamaterials for electrically triggered multifunctional control. *Nat Commun*. (2016) **7**:13236. doi: 10.1038/ncomms13236
94. Cai HL, Chen S, Zou CW, Huang QP, Liu Y, Hu X, et al. Multifunctional hybrid metasurfaces for dynamic tuning of terahertz waves. *Adv Optical Mater*. (2018) **6**:1800257. doi: 10.1002/adom.201800257
95. Cuo JY, Wang T, Zhao H, Wang XK, Feng SF, Han P, et al. Reconfigurable terahertz metasurface pure phase holograms. *Adv Optical Mater*. (2019) **7**:1801696. doi: 10.1002/adom.201801696
96. She A, Zhang SY, Shian S, Clarke DR, Capasso F, et al. Adaptive metalenses with simultaneous electrical control of focal length astigmatism and shift. *Sci Adv*. (2018) **4**:eaap9957. doi: 10.1126/sciadv.aap9957
97. Giovampola CD, Engheta N. Digital metamaterials. *Nat Mater*. (2014) **13**:1115–21. doi: 10.1038/nmat4082
98. Cui TJ, Qi MQ, Wan X, Zhao J, Cheng Q. Coding metamaterials, digital metamaterials and programmable metamaterials. *Light Sci Appl*. (2014) **3**:e218. doi: 10.1038/lsa.2014.99
99. Liu S, Noor A, Du LL, Zhang L, Xu Q, Luan K, et al. Anomalous refraction and non-diffractive Bessel-beam generation of terahertz waves through transmission-type coding metasurfaces. *ACS Photon*. (2016) **3**:1968–77. doi: 10.1021/acsp Photonics.6b00515
100. Liang LJ, Qi MQ, Yang J, Shen XP, Zhai JQ, Xu WZ, et al. Anomalous terahertz reflection and scattering by flexible and conformal coding metamaterials. *Adv Optical Mater*. (2015) **3**:1374–80. doi: 10.1002/adom.201500206
101. Gao LH, Cheng Q, Yang J, Ma SJ, Zhao J, Liu S, et al. Broadband diffusion of terahertz waves by multi-bit coding metasurfaces. *Light Sci Appl*. (2015) **4**:e324. doi: 10.1038/lsa.2015.97
102. Liu S, Cui TJ, Zhang L, Xu Q, Wang Q, Wan X, et al. Convolution operations on coding metasurface to reach flexible and continuous controls of terahertz beams. *Adv Sci*. (2016) **3**:1600156. doi: 10.1002/adv.201600156
103. Yang MS, Yan X, Zhang Z, Gao J, Liang LJ, Guo XY, et al. Ultra-wideband low-loss control of terahertz scatterings via an all-dielectric coding metasurface. *ACS Appl Electron Mater*. (2020) **2**:1122–9. doi: 10.1021/acsaem.0c00107
104. Liu S, Cui TJ, Xu Q, Bao D, Du LL, Wan X, et al. Anisotropic coding metamaterials and their powerful manipulation of differently polarized terahertz waves. *Light Sci Appl*. (2016) **5**:e16076. doi: 10.1038/lsa.2016.76
105. Liu S, Zhang L, Yang QL, Xu Q, Yang Y, Noor A, et al. Frequency-dependent dual-functional coding metasurfaces at terahertz frequencies. *Adv Optical Mater*. (2016) **4**:1965–73. doi: 10.1002/adom.201600471
106. Li LL, Cui TJ, Ji W, Liu S, Ding J, Wan X, et al. Electromagnetic reprogrammable coding-metasurface holograms. *Nat Commun*. (2017) **8**:1–7. doi: 10.1038/s41467-017-00164-9

107. Li LL, Ruan HX, Liu C, Li Y, Shuang Y, Alu A, et al. Machine-learning reprogrammable metasurface imager. *Nat Commun.* (2019) **10**:1–8. doi: 10.1038/s41467-019-09103-2
108. Zhang L, Chen XQ, Liu S, Zhang Q, Zhao J, Dai JY, et al. Space-time-coding digital metasurfaces. *Nat Commun.* (2018) **9**:1–11. doi: 10.1038/s41467-018-06802-0
109. Zhao J, Yang X, Dai JY, Cheng Q, Li X, Qi NH, et al. Programmable time-domain digital-coding metasurface for non-linear harmonic manipulation and new wireless communication systems. *Nat Sci Rev.* (2019) **6**:231–8. doi: 10.1093/nsr/nwy135
110. Cui TJ, Liu S, Bai GD, Ma Q. Direct transmission of digital message via programmable coding metasurface. *Research.* (2019) **2019**:2584509. doi: 10.34133/2019/2584509
111. Rouhi K, Rajabalipanah H, Abdolali A. Multi-bit graphene-based bias-encoded metasurfaces for real-time terahertz wavefront shaping from controllable orbital angular momentum generation toward arbitrary beam tailoring. *Carbon.* (2019) **149**:125–38. doi: 10.1016/j.carbon.2019.04.034
112. Rouhi K, Rajabalipanah H, Abdolali A. Real-time and broadband terahertz wave scattering manipulation via polarization-insensitive conformal graphene-based coding metasurfaces. *Ann Phys.* (2018) **530**:1700310. doi: 10.1002/andp.201700310
113. Zhang Z, Yan X, Liang LJ, Wei DQ, Wang M, Wang YR, et al. The novel hybrid metal-graphene metasurfaces for broadband focusing and beam-steering in farfield at the terahertz frequencies. *Carbon.* (2018) **132**:529–38. doi: 10.1016/j.carbon.2018.02.095
114. Momeni A, Rouhi K, Rajabalipanah H, Abdolali A. An information theory-inspired strategy for design of re-programmable encrypted graphene-based coding metasurfaces at terahertz frequencies. *Sci Rep.* (2018) **8**:6200. doi: 10.1038/s41598-018-24553-2
115. Kim M, Jeong J, Poon JKS, Eleftheriades GV, et al. Vanadium-dioxide-assisted digital optical metasurfaces for dynamic wavefront engineering. *J Opt Soc Am B.* (2016) **33**:980–8. doi: 10.1364/josab.33.000980
116. Li J, Zhang YT, Li JN, Yan X, Liang LJ, Zhang Z, et al. Amplitude modulation of anomalously reflected terahertz beams using all-optical active pancharatnam–berry coding metasurfaces. *Nanoscale.* (2019) **11**:5746–53. doi: 10.1039/c9nr00675c
117. Hosseininejad SE, Rouhi K, Neshat M, Faraji-Dana R, Cabellos-Aparicio A, Abadal S, et al. Reprogrammable graphene-based metasurface mirror with adaptive focal point for THz imaging. *Sci Rep.* (2019) **9**:2868. doi: 10.1038/s41598-019-39266-3
118. Rajabalipanah H, Abdolali A, Rouhi K. Reprogrammable spatiotemporally modulated graphene-based functional metasurfaces. *IEEE J Emerg Sel Topics Power Electron.* (2020) **10**:75–87. doi: 10.1109/jetcas.2020.2972928
119. Manjappa M, Pitchappa P, Singh N, Wang N, Zheludev NI, Lee CK, et al. Reconfigurable MEMS Fano metasurfaces with multiple-input–output states for logic operations at terahertz frequencies. *Nat Commun.* (2018) **9**:4056. doi: 10.1038/s41467-018-06360-5
120. Cong L, Pitchappa P, Wang N, Singh R. Electrically programmable terahertz diatomic metamolecules for chiral optical control. *Research.* (2019) **2019**:7084251. doi: 10.34133/2019/7084251
121. Ho CP, Pitchappa P, Lee CK. Digitally reconfigurable binary coded terahertz metamaterial with output analogous to NOR and AND. *J Appl Phys.* (2016) **119**:153104. doi: 10.1063/1.4946891
122. Pitchappa P, Ho CP, Cong LQ, Singh R, Singh N, Lee CK. Reconfigurable digital metamaterial for dynamic switching of terahertz anisotropy. *Adv Optical Mater.* (2016) **4**:391–8. doi: 10.1002/adom.201500588
123. Tamagnone M, Capdevila S, Lombardo A, Wu J, Centeno A, Zurutuza A, et al. Graphene reflectarray metasurface for terahertz beam steering and phase modulation. *Condens. Matter Phys.* To be published.
124. Wu JB, Shen Z, Ge SJ, Chen BW, Shen ZX, Wang TF, et al. Liquid crystal programmable metasurface for terahertz beam steering. *Appl Phys Lett.* (2020) **116**:131104. doi: 10.1063/1.5144858
125. Fu XJ, Yang F, Liu CX, Wu XJ, Cui TJ. Terahertz beam steering technologies: from phased arrays to field-programmable metasurfaces. *Adv Optical Mater.* (2019) **8**:1900628. doi: 10.1002/adom.201900628
126. Chen HT, Taylor AJ, Yu NF. A review of metasurfaces: physics and applications. *Rep Prog Phys.* (2016) **79**:076401. doi: 10.1088/0034-4885/79/7/076401
127. Fan K, Padilla WJ. Dynamic electromagnetic metamaterials. *Mater Today.* (2015) **18**:39–50. doi: 10.1016/j.mattod.2014.07.010
128. Cui TJ, Liu S, Zhang L. Information metamaterials metasurfaces. *J Mater Chem C.* (2017) **5**:3644–68. doi: 10.1039/C7TC00548B
129. Bao L, Cui TJ. Tunable, reconfigurable, programmable metamaterials. *Micro Opt Technol Lett.* (2019) **62**:9–32. doi: 10.1002/mop.32164
130. Piesiewicz R, Kleine-Ostmann T, Krumbholz N, Mittleman D, Koch M, Schobel J, et al. Short-range ultra-broadband terahertz communications: concepts and perspectives. *IEEE Antennas Propag Mag.* (2007) **49**:24–39. doi: 10.1109/map.2007.4455844
131. Lepeshov S, Gorodetsky A, Krasnok A, Toropov N, Vartanyan TA, Belov P, et al. Boosting terahertz photoconductive antenna performance with optimised plasmonic nanostructures. *Sci Rep.* (2018) **8**:6624. doi: 10.1038/s41598-018-25013-7
132. Hashemi MR, Cakmakyapan S, Jarrahi M. Reconfigurable metamaterials for terahertz wave manipulation. *Rep Prog Phys.* (2017) **80**:094501. doi: 10.1088/1361-6633/aa77cb

Conflict of Interest: The authors declare that the research was conducted in the absence of any commercial or financial relationships that could be construed as a potential conflict of interest.

Copyright © 2020 Tian, Shen, Zhang, Li, Jiang and Cui. This is an open-access article distributed under the terms of the Creative Commons Attribution License (CC BY). The use, distribution or reproduction in other forums is permitted, provided the original author(s) and the copyright owner(s) are credited and that the original publication in this journal is cited, in accordance with accepted academic practice. No use, distribution or reproduction is permitted which does not comply with these terms.